PERGAMON

International Journal of Solids and Structures 40 (2003) 1001–1031

INTERNATIONAL JOURNAL OF SOLIDS and STRUCTURES

www.elsevier.com/locate/ijsolstr

# Boundary eigensolutions in elasticity II. Application to computational mechanics

A.R. Hadjesfandiari, G.F. Dargush *

*Department of Civil Engineering, State University of New York at Buffalo, 135 Ketter Hall, North Campus, Buffalo, NY 14260, USA*

Received 21 February 2000; received in revised form 9 October 2002

**Abstract**

The theory of fundamental boundary eigensolutions for elastostatic problems, developed in Part I, is applied to formulate methods for computational mechanics. This theory shows that every elastic solution can be written as a linear combination of some fundamental boundary orthogonal deformations, thus providing a generalized Fourier expansion. One finds that traditional boundary element and finite element methods are largely consistent with this theory, but do not harness its full power. This theory shows that these computational methods are indirectly a generalized discrete Fourier analysis. Furthermore, by utilizing suitable boundary weight functions, boundary element and finite element formulations may be written exclusively in terms of bounded quantities, even for non-smooth problems involving notches, cracks, mixed boundary conditions and bi-material interfaces. The close relationship between the resulting boundary element and finite element methods also becomes evident. Both use displacement and surface traction as primary variables. A new degree-of-freedom concept is introduced, along with a stiffness tensor that enables one to visualize a finite element method via a boundary discretization process, just as in a boundary element approach. Global convergence characteristics of the traction-oriented finite element method are also developed. Comparisons with closed-form fundamental boundary eigensolutions for a circular elastic disc are presented in order to provide a means for assessing the numerical methods. Several other numerical examples are solved efficiently by using the concept of boundary eigensolutions in an indirect fashion. The results indicate that the algorithms follow the underlying theory and that solutions to non-smooth problems can be obtained in a systematic manner. Beyond this, the concept of boundary eigensolutions provides an alternative view of computational continuum mechanics that may lead to the development of other non-traditional approaches.


*Keywords:* Elasticity; Computational mechanics; Boundary

## 1. Introduction

The general theory of fundamental boundary eigensolutions for elastostatic boundary value problems was presented in Part I (Hadjesfandiari and Dargush, 2001a). Here we apply this theory to computational

* Corresponding author. Tel.: +1-716-645-2114; fax: +1-716-645-3733.
*E-mail address:* gdargush@eng.buffalo.edu (G.F. Dargush).

0020-7683/02/$ - see front matter © 2002 Elsevier Science Ltd. All rights reserved.
PII: S0020-7683(02)00586-3

mechanics, and more specifically to the further development of boundary element and finite element methods for elastic bodies. Related work on the scalar potential problem is provided in Hadjesfandiari and Dargush (2001b,c) and in Hadjesfandiari (1998). The latter reference also includes initial work on the elastostatic problem.

The major traditional methods of computational mechanics do not have a common means to enforce boundary conditions. For an elastic boundary value problem, the traditional finite element method uses lumped nodal forces to model the tractions in a very approximated manner, but as a result generates a symmetric stiffness matrix. On the other hand, the standard boundary element method uses tractions as primary variables, but generates non-symmetric matrices. Under certain circumstances, these non-symmetric matrices can cause instability in the solutions. The theory of fundamental boundary eigensolutions as developed here shows that these computational methods are indirectly a *generalized discrete Fourier analysis*. This not only gives a new common view to both methods, but also directs us in modifying these methods and in understanding the source of some ill-behavior.

Our attention in this paper will be focused primarily on the development of boundary element and finite element methods that are completely consistent with the theory of elastostatic boundary value problems, including all of those problems that are classified as non-smooth. Examples of non-smooth problems include those involving notches, cracks, mixed boundary conditions and certain bi-material interfaces. We will show that the resulting computational methods are indirectly a generalized discrete Fourier analysis. The introduction of a weight function simply alters the underlying orthogonal basis functions, thus enabling us to solve non-smooth problems systematically.

Of course, many researchers over the years have developed numerical approaches for the solutions of non-smooth boundary value problems. Barsoum (1975) and Henshell and Shaw (1975) devised quarter-point finite elements for linear elastic fracture mechanics analysis, while others have proposed finite element methods based on Bueckner weight functions (Bueckner, 1970; Paris et al., 1976) for similar problems. Snyder and Cruse (1975) first applied boundary integral equation methods to a fracture problem by using specialized fundamental solutions. More recently, Blandford et al. (1981) developed quarter-point and traction-singular elements within an integral equation framework. However, these approaches are difficult to extend to more general non-smooth problems. Traditional finite element methods that utilize the nodal force concept are particularly problematic.

Work on the general non-smooth boundary value problem is more limited. Barone and Robinson (1972) solved problems involving elastic bodies with notches by combining locally defined singular eigenfunctions within an integral equation approach. Singularity subtraction methods have also been proposed by Symm (1973) for the potential problem and later by Aliabadi et al. (1987) for elasticity. Typically these subtraction methods introduce auxiliary equations in order to solve for the coefficients of the singular solutions.

The approach to be developed here, based upon the theory of fundamental boundary eigensolutions, allows a more systematic treatment of non-smooth problems and also provides a deeper unity between the theory of elastic boundary value problems and its computational mechanics representation. Interestingly, the stress analysis of bodies with notches or bi-material interfaces has become more important in recent years as some research indicates that the general stress intensity factors are controlling parameters for failure. These ideas are developed in Dunn et al. (1997) for notched bodies and in Reedy and Guess (1997) for bi-material interfaces.

We should emphasize, however, that the theory of fundamental boundary eigensolutions is not only a tool to provide a systematic approach to solve non-smooth problems. More importantly the theory enables researchers to look at the finite element method and the boundary element method from the same mathematical view, i.e., as indirect generalized discrete Fourier methods. The theory explains the character of the system matrices, and the boundary eigensolutions derived from the matrices provide a real basis for the solution of boundary value problems. This result is more striking for the boundary element method in which the matrices are in general non-symmetric. Fortunately, we may utilize the theory of boundary

eigensolutions to formulate new computational methods, but in most cases we will not need to explicitly determine the eigenmodes. However by constructing this theory, we may obtain a new perspective for computational mechanics and a deeper connection with many ideas from classical mathematics. We also believe that this approach provides a powerful tool for the further development of computational methods.

With this in mind, we provide a brief review of the theory of boundary eigensolutions in the following section. A new boundary element formulation that can systematically address the singularities associated with non-smooth problems is then presented in Section 3. Afterward we develop a traction-oriented finite element method in Section 4 and show its relation to the previous boundary element formulation. In both methods, the theory of fundamental boundary eigensolutions plays a key role. Results from a series of numerical examples are presented in Section 5. Included are correlations with the closed-form eigensolutions for an elastic circular disc and investigations on the performance of the proposed boundary element and finite element methods for problems involving mixed boundary conditions, notches, cracks and a bi-material interface. Finally, Section 6 provides some concluding remarks.

## 2. Theory of fundamental boundary eigensolutions

A theory of fundamental boundary eigensolutions for elastostatic boundary value problems was developed in Part I (Hadjesfandiari and Dargush, 2001a). As we saw, the *fundamental boundary eigenproblem* for elastostatics can be defined as follows:

Find the non-trivial displacement $\boldsymbol{u}$ such that in the domain $V$

$$\sigma_{ij,j} = C_{ijkl} u_{k,lj} = 0 \tag{2.1a}$$

and on the boundary $S$

$$t_i = \lambda \varphi_{ij} u_j \tag{2.1b}$$

In (2.1), $\boldsymbol{\sigma}$, $\boldsymbol{t}$ and $\boldsymbol{C}$, represent the stress tensor, traction vector and elastic constitutive tensor, respectively, while $\lambda$ is the eigenparameter. Furthermore $\boldsymbol{\Phi}$ is a positive definite, integrable tensorial weight function defined on the boundary $S$. Notice that this definition permits $\varphi_{ij}$ to be discontinuous and even singular at some points.

Unlike traditional eigenproblems, which introduce the eigenvalue in the governing differential equation, here the eigenvalue $\lambda$ appears in the boundary condition. This difference provides an entirely new way to view the solutions of elastostatic problems and the associated computational mechanics methods.

From the fundamental boundary condition (2.1b), we note that the traction $\boldsymbol{t}$ is always continuous on the boundary when $\boldsymbol{\Phi}$ is continuous, even if there are geometrically non-smooth points (e.g., edges, corners).

The eigensolutions of (2.1) have a number of interesting and useful properties that are developed in Part I. The most important properties include the reality of eigensolutions, completeness and orthogonality of eigenmodes $\boldsymbol{u}^{(n)}$ with respect to $\boldsymbol{\Phi}$ as

$$\int_S \varphi_{ij} u_i^{(m)} u_j^{(n)} \, \mathrm{d}S = \delta_{mn} \tag{2.2}$$

where $\delta_{mn}$ is the Kronecker delta. More elegantly, one can conclude that the metric space of fundamental eigenmodes is a Hilbert space.

As a result, these fundamental eigensolutions provide a basis for solutions to elastostatic boundary value problems in the form of generalized Fourier series or fundamental eigenexpansion

$$\boldsymbol{u} = \sum_{n=1}^{\infty} A_n \boldsymbol{u}^{(n)} \quad \text{in } V \cup S \tag{2.3}$$

and on the boundary

$$\boldsymbol{t} = \boldsymbol{\Phi} \cdot \sum_{n=1}^{\infty} A_n \lambda_n \boldsymbol{u}^{(n)} \quad \text{on } S \tag{2.4}$$

with

$$A_n = \int_S \boldsymbol{u} \cdot \boldsymbol{\Phi} \cdot \boldsymbol{u}^{(n)} \, \mathrm{d}S \tag{2.5}$$

for orthonormal eigenmodes.

As we mentioned in Part I, the eigenmodes with respect to $\varphi_{ij} = \delta_{ij}$ are analytic even on the boundary. Although this is a nice mathematical property, it is not very useful for solving non-smooth problems in computational mechanics. We will see that the traditional boundary element method attempts to follow this expansion based on these analytic eigenmodes with respect to $\varphi_{ij} = \delta_{ij}$. This is why we cannot consider singularity systematically. Additionally, it should be remembered that in traditional finite element formulations the nodal force concept is introduced to approximate the traction. As a result, the traditional finite element method does not exactly follow the theory of fundamental eigenexpansion, even with $\varphi_{ij} = \delta_{ij}$.

We assume that in physical problems $\boldsymbol{u}$ is continuous everywhere, but that $\boldsymbol{t}$ can be piecewise continuous. This allows $\boldsymbol{t}$ to exhibit discontinuities, and even singularities. With the present approach, we attempt to choose $\boldsymbol{\Phi}$ such that the weighted traction $\boldsymbol{t}^{\varphi}$ is piecewise regular. Thus $\boldsymbol{t}^{\varphi}$, defined by the relation

$$t_i = \varphi_{ij} t_j^{\varphi}$$

still may have discontinuities, but it now remains bounded everywhere on $S$. Then, the expansion for $\boldsymbol{t}^{\varphi}$ is

$$\boldsymbol{t}^{\varphi} = \sum_{n=1}^{\infty} A_n \lambda_n \boldsymbol{u}^{(n)} \quad \text{on } S \tag{2.6}$$

If the deformation $\boldsymbol{u}$ is such that the weighted traction $\boldsymbol{t}^{\varphi}$ is piecewise regular on the boundary $S$, then the generalized Fourier series (2.6) converges at each point $x$ on the boundary $S$ to the principal mean value $\hat{\boldsymbol{t}}^{\varphi}$ (Part I, Appendix B). Furthermore, the expansions (2.3) and (2.6) both converge in the mean because $\boldsymbol{u}$ and $\boldsymbol{t}^{\varphi}$ are mean square integrable functions (i.e., $L_2$-functions) with respect to $\boldsymbol{\Phi}$. Consequently, the partial expansions

$$\boldsymbol{u}_N = \sum_{n=1}^{N} A_n \boldsymbol{u}^{(n)} \quad V \cup S \tag{2.7}$$

$$\boldsymbol{t}_N^{\varphi} = \sum_{n=1}^{N} A_n \lambda_n \boldsymbol{u}^{(n)} \quad \text{on } S \tag{2.8}$$

with Fourier coefficients defined in (2.5) approximate the exact quantities in such a way that

$$\|\boldsymbol{u} - \boldsymbol{u}_N\|^2 = \int_S \varphi_{ij}(u_i - u_{iN})(u_j - u_{jN}) \, \mathrm{d}S \tag{2.9}$$

$$\|\boldsymbol{t}^{\varphi} - \boldsymbol{t}_N^{\varphi}\|^2 = \int_S \varphi_{ij}(t_i^{\varphi} - t_{iN}^{\varphi})(t_j^{\varphi} - t_{jN}^{\varphi}) \, \mathrm{d}S = \int_S (t_i^{\varphi} - t_{iN}^{\varphi})(t_i - t_{iN}) \, \mathrm{d}S \tag{2.10}$$

are minimum. This provides a global criterion for convergence.

Convergence of $\boldsymbol{t}_N^{\varphi}$ to $\boldsymbol{t}^{\varphi}$ is not uniform wherever there is a discontinuity in $\boldsymbol{t}^{\varphi}$. From analysis we know $\boldsymbol{t}_N^{\varphi}$ is a continuous function on the boundary. If $N$ approaches infinity, the summation can be discontinuous and capture the discontinuity of the weighted traction $\boldsymbol{t}^{\varphi}$. For finite $N$, we have Gibbs' phenomenon, illustrated by oscillations of $\boldsymbol{t}_N^{\varphi}$ near to the discontinuity.

The displacement $\boldsymbol{u}$ is an analytic function in the domain $V$. It is also continuous on the boundary for an acceptable physical problem. This allows $\boldsymbol{u}$ to be non-analytic at some boundary points in two dimensional domains or on some boundary lines and points in three-dimensional problems. The degree of continuity of $\boldsymbol{u}$ determines the speed of decrease of $A_n$ for higher modes. The coefficients $A_n$ decrease faster when the function $\boldsymbol{t}^{\varphi}$ is more smooth. When $\boldsymbol{t}^{\varphi}$ has a discontinuity at one or more points, the speed at which the coefficients decrease is slower. This means that the contribution of higher modes is more important.

With this background in mind, integral equation methods and variational methods can now be developed that are consistent with the theory of elastic boundary value problems. The development of these methods, along with their corresponding numerical implementations, will provide the main focus for the remainder of this paper. Boundary element formulations are considered in the next section.

## 3. Boundary element methods

### 3.1. Formulation

The boundary integral representation for the elastostatic problem without body force can be written (Part I)

$$c_{ij}(\xi)u_j(\xi) + \int_S \mathscr{F}_{ij}(\xi,x)u_j(x)\,\mathrm{d}S(x) = \int_S \mathscr{G}_{ij}(\xi,x)t_j(x)\,\mathrm{d}S(x) \tag{3.1}$$

where $\mathscr{G}(x,\xi)$ and $\mathscr{F}(x,\xi)$ are the elasticity kernels and $\boldsymbol{c}(\xi)$ is a tensor that characterizes the local geometry at $\xi$. By substituting the fundamental boundary condition $t_j(x) = \lambda\varphi_{jk}(x)u_k(x)$ into (3.1), we obtain the fundamental eigenproblem in integral form as

$$c_{ij}(\xi)u_j(\xi) + \int_S \mathscr{F}_{ij}(\xi,x)u_j(x)\,\mathrm{d}S(x) = \lambda\int_S \mathscr{G}_{ij}(\xi,x)\varphi_{jk}(x)u_k(x)\,\mathrm{d}S(x) \tag{3.2}$$

This problem has an infinite number of eigensolutions $(\lambda_n, \boldsymbol{u}^{(n)})$ which are boundary orthogonal with respect to $\boldsymbol{\Phi}$.

In terms of $\boldsymbol{u}$ and $\boldsymbol{t}^{\varphi}$, the boundary integral representation (3.1) reduces to

$$c_{ij}(\xi)u_j(\xi) + \int_S \mathscr{F}_{ij}(\xi,x)u_j(x)\,\mathrm{d}S(x) = \int_S \mathscr{G}_{ij}(\xi,x)\varphi_{jk}(x)t_k^{\varphi}(x)\,\mathrm{d}S(x) \tag{3.3}$$

It is seen that when $\varphi_{ij} = \delta_{ij}$, (3.3) reduces to (3.1).

### 3.2. Numerical implementation

In practice for arbitrary domains, we may solve (3.3) numerically via a boundary element method (e.g., Banerjee, 1994). By discretizing the boundary into a finite number $N_E$ of elements, utilizing low-order polynomial shape functions within the elements and collocating at the nodes, we obtain a system of algebraic equations that can be written

$$\boldsymbol{F}\boldsymbol{U} = \boldsymbol{G}^{\varphi}\boldsymbol{T}^{\varphi} \tag{3.4}$$

where $\boldsymbol{U}$ and $\boldsymbol{T}^{\varphi}$ represent nodal values of displacement and weighted traction, respectively, while $\boldsymbol{F}$ and $\boldsymbol{G}^{\varphi}$ are system matrices formed through an assembly process. Thus, symbolically

$$\boldsymbol{F} = \sum_{e=1}^{N_{\mathrm{E}}} \int_{S} \boldsymbol{F}(\xi, x)\boldsymbol{N}^{(e)}(x)\,\mathrm{d}S(x) \tag{3.5a}$$

$$\boldsymbol{G}^{\varphi} = \sum_{e=1}^{N_{\mathrm{E}}} \int_{S} \boldsymbol{G}(\xi, x)\cdot\boldsymbol{\Phi}(x)\boldsymbol{N}^{(e)}(x)\,\mathrm{d}S(x) \tag{3.5b}$$

where $\boldsymbol{N}^{(e)}(x)$ is the matrix of shape functions associated with element number $e$.

In the present work, the integrations required to form the $\boldsymbol{G}^{\varphi}$ and $\boldsymbol{F}$ matrices are performed analytically, where possible, or by utilizing gaussian quadrature within an adaptive subsegmentation algorithm. The diagonal elements of $\boldsymbol{F}$ are evaluated indirectly by satisfying rigid body translations.

In the new formulation (3.4) for non-smooth problems, $\boldsymbol{\Phi}$ generally increases the singularity of the integration for $\boldsymbol{G}^{\varphi}$. However, for physically relevant problems the integrand always remains weakly singular. For two-dimensional problems this integration can be transformed to traditional form by introducing a suitable mapping. Alternatively gaussian quadrature formulas with non-classical weights can be developed, following procedures outlined in Press et al. (1992). This latter approach was employed for the numerical results presented in Section 5. Additionally, we utilize non-traditional shape functions for displacement variation in elements adjacent to the non-smooth points in order to capture the local behavior more accurately.

Obviously, when $\varphi_{ij} = \delta_{ij}$ we have $\boldsymbol{G}^{\varphi} = \boldsymbol{G}$ where $\boldsymbol{G}$ is the matrix that appears in the standard boundary element method. Then

$$\boldsymbol{F}\boldsymbol{U} = \boldsymbol{G}\boldsymbol{T} \tag{3.6}$$

where $\boldsymbol{T}$ represents the nodal values of traction. In this case, traditional shape functions are used to represent the displacement and traction over all boundary elements.

By using the fundamental boundary conditions, the boundary element version of the fundamental boundary eigenproblem is

$$\boldsymbol{F}\boldsymbol{U} = \lambda\widehat{\boldsymbol{G}}^{\varphi}\boldsymbol{U} \tag{3.7}$$

While $\boldsymbol{G}^{\varphi}$ in (3.4) is in general a rectangular matrix to allow for discontinuity in weighted traction $\boldsymbol{T}^{\varphi}$, the matrix $\widehat{\boldsymbol{G}}^{\varphi}$ for the eigenproblem (3.7) is a square version of $\boldsymbol{G}^{\varphi}$ due to the continuity requirement inherent in the fundamental boundary condition

$$\boldsymbol{T}^{\varphi} = \lambda\boldsymbol{U}$$

Furthermore, it should be noted that the translational rigid body eigenmodes corresponding to $\lambda = 0$ are automatically satisfied due to the indirect evaluation of the diagonal elements of $\boldsymbol{F}$.

As mentioned in Section 2, we expect real eigensolutions of the fundamental problem. Additionally, we expect boundary orthogonality of the eigenmodes with respect to $\boldsymbol{\Phi}$ in closed-form (2.2). In discretized form this becomes

$$\int_{S} \boldsymbol{U}^{(m)\mathrm{T}}\boldsymbol{N}^{\mathrm{T}}\boldsymbol{\Phi}\boldsymbol{N}\boldsymbol{U}^{(n)}\,\mathrm{d}S = 0 \quad \text{for } m \neq n$$

or simply

$$\boldsymbol{U}^{(m)\mathrm{T}}\widehat{\boldsymbol{S}}^{\varphi}\boldsymbol{U}^{(n)} = 0 \quad \text{for } m \neq n \tag{3.8}$$

where

$$\widehat{\boldsymbol{S}}^{\varphi} = \int_S \boldsymbol{N}^{\mathrm{T}}\boldsymbol{\Phi}\boldsymbol{N}\,\mathrm{d}S \tag{3.9}$$

with shape function matrix $\boldsymbol{N}(x)$. Since $\widehat{\boldsymbol{S}}^{\varphi}$ depends on the boundary discretization and weight function $\boldsymbol{\Phi}$ we call it the *weighted boundary matrix*. From (3.8), we expect the eigenvectors to be orthogonal with respect to $\widehat{\boldsymbol{S}}^{\varphi}$. Note that $\widehat{\boldsymbol{S}}^{\varphi}$ is a square matrix of the same size as $\widehat{\boldsymbol{G}}^{\varphi}$.

For a boundary element system with $N_{\mathrm{B}}$ boundary nodes, the approximate solution can be written as

$$\tilde{\boldsymbol{u}} = \sum_{n=1}^{N} \tilde{A}_n \tilde{\boldsymbol{u}}_n \tag{3.10}$$

where $\tilde{\boldsymbol{u}}_n$ and $\tilde{A}_n$ are approximate eigenmodes and generalized Fourier coefficients, respectively, and $N = dN_{\mathrm{B}}$ with $d$ representing the number of spatial dimensions.

At the nodes

$$\widetilde{\boldsymbol{U}} = \sum_{n=1}^{N} \tilde{A}_n \widetilde{\boldsymbol{U}}^{(n)} \tag{3.11}$$

and then, assuming orthogonality with respect to $\widehat{\boldsymbol{S}}^{\varphi}$, for the approximate Fourier coefficients we have

$$\tilde{A}_n = \frac{\widetilde{\boldsymbol{U}}^{\mathrm{T}}\widehat{\boldsymbol{S}}^{\varphi}\widetilde{\boldsymbol{U}}^{(n)}}{\widetilde{\boldsymbol{U}}^{(n)\mathrm{T}}\widehat{\boldsymbol{S}}^{\varphi}\widetilde{\boldsymbol{U}}^{(n)}} \tag{3.12}$$

In closed-form, we expect real boundary orthogonal eigensolutions of the generalized fundamental problem. However, after discretization both $\boldsymbol{F}$ and $\widehat{\boldsymbol{G}}^{\varphi}$ are in general non-symmetric matrices. As a result, these desirable characteristics cannot be guaranteed for the collocation-based boundary element eigensolutions. This is why we did not normalize the Fourier coefficients in (3.12) which might be complex. The instability of the boundary element method in some cases in elastostatics is due to the presence of complex eigensolutions.

For moderately sized problems, the real, non-symmetric generalized eigensolver available in the LAPACK package (Anderson et al., 1992) can be used to extract the eigenvalues and eigenvectors of (3.7), some of which may be complex. In any case, these eigensolutions are fundamental to the discretized representation of the elastostatic problem in the domain $V$ with boundary $S$. Solutions of (3.4) can be expressed in terms of the eigenvectors. By refining the boundary element mesh, we increase the number of basis functions and also tend to improve the accuracy of the lower eigensolutions.

It should be emphasized that we need not actually solve the fundamental eigenproblem (3.7) in order to find the solution to a boundary value problem associated with (3.1) or its discrete version (3.4). Numerical solutions of the collocation-based direct boundary element equations for elastostatics were obtained several decades ago (Rizzo, 1967; Cruse, 1969). We now recognize, however, that the direct solution of (3.4) implicitly utilizes the fundamental eigenvectors $\boldsymbol{U}^{(n)}$ as its basis. Thus, we can obtain a better understanding of the $\boldsymbol{F}$ and $\boldsymbol{G}^{\varphi}$ matrices by studying the fundamental eigenproblem, and some of the strengths and limitations of present boundary element methods can be examined from this new perspective. We should also mention that despite the long history of the method in elasticity, this represents the first spectral analysis of the direct boundary element method.

## 4. Finite element methods

### 4.1. Formulation

In order to develop a finite element method for elastostatic problems that is consistent with the theory of fundamental eigensolutions, we begin with the variational formulations presented in Part I. The Rayleigh quotient can be written

$$R(\boldsymbol{u}) = \lambda = \frac{\int_V C_{ijkl}\varepsilon_{ij}\varepsilon_{kl}\,\mathrm{d}V}{\int_S \varphi_{ij}u_i u_j\,\mathrm{d}S} \tag{4.1}$$

By subdividing the domain and boundary into finite elements and boundary elements, respectively, we obtain the discretized form of the Rayleigh quotient as

$$R(\boldsymbol{U}) = \frac{\boldsymbol{U}^{\mathrm{T}}\boldsymbol{K}\boldsymbol{U}}{\boldsymbol{U}^{\mathrm{T}}\widehat{\boldsymbol{S}}^{\varphi}\boldsymbol{U}} \tag{4.2}$$

where $\boldsymbol{K}$ is the usual stiffness matrix (e.g., Bathe, 1996) and $\widehat{\boldsymbol{S}}^{\varphi}$ is again the weighted boundary matrix defined by (3.9).

It was proved in Part I that the Rayleigh quotient is an extremum when $\boldsymbol{u}$ is a generalized boundary eigenmode and that $R[\boldsymbol{u}_n] = \lambda_n$. In discretized form, the functional $R[\boldsymbol{U}]$ must be extremum at the corresponding eigenvectors. By taking the first variation of (4.2), we have

$$\delta R(\boldsymbol{U}) = 2\frac{(\delta\boldsymbol{U}^{\mathrm{T}}\boldsymbol{K}\boldsymbol{U})(\boldsymbol{U}^{\mathrm{T}}\widehat{\boldsymbol{S}}^{\varphi}\boldsymbol{U}) - (\delta\boldsymbol{U}^{\mathrm{T}}\widehat{\boldsymbol{S}}^{\varphi}\boldsymbol{U})(\boldsymbol{U}^{\mathrm{T}}\boldsymbol{K}\boldsymbol{U})}{(\boldsymbol{U}^{\mathrm{T}}\widehat{\boldsymbol{S}}^{\varphi}\boldsymbol{U})^2} = 0 \tag{4.3}$$

or

$$\delta\boldsymbol{U}^{\mathrm{T}}[\boldsymbol{K}\boldsymbol{U} - R[\boldsymbol{U}]\widehat{\boldsymbol{S}}^{\varphi}\boldsymbol{U}] = 0 \tag{4.4}$$

However, since $\delta\boldsymbol{U}$ is arbitrary, the following relation is obtained at an extremum

$$\boldsymbol{K}\boldsymbol{U} = \lambda\begin{Bmatrix} \widehat{\boldsymbol{S}}^{\varphi}\boldsymbol{U} \\ \boldsymbol{0} \end{Bmatrix} \tag{4.5}$$

with $R[\boldsymbol{U}^{(n)}] = \lambda_n$ and the right-hand side partitioned into boundary and interior nodes. Equation (4.5) is the generalized fundamental eigenproblem in discretized variational form. It is thus an alternative to the boundary element eigenproblem expressed in (3.7).

Furthermore, (4.5) suggests that a finite element formulation for boundary value problems should be defined as

$$\boldsymbol{K}\boldsymbol{U} = \begin{Bmatrix} \boldsymbol{S}^{\varphi}\boldsymbol{T}^{\varphi} \\ \boldsymbol{0} \end{Bmatrix} \tag{4.6}$$

where $\boldsymbol{S}^{\varphi}$ is the rectangular version of $\widehat{\boldsymbol{S}}^{\varphi}$, to allow discontinuity in $\boldsymbol{T}^{\varphi}$.

This formulation can be derived from the principle of virtual work or weak formulation presented in Part I

$$\int_V \sigma_{ij}\delta\varepsilon_{ij}\,\mathrm{d}V = \int_S \varphi_{ij}t_j^{\varphi}\delta u_i\,\mathrm{d}S \tag{4.7}$$

By inserting the fundamental boundary condition $t_j^{\varphi} = \lambda u_j$, we have

$$\int_V \sigma_{ij}\delta\varepsilon_{ij}\,\mathrm{d}V = \lambda \int_S \varphi_{ij}u_j\delta u_i\,\mathrm{d}S \tag{4.8}$$

This latter equation is the weak formulation for the fundamental boundary eigensolutions. Both variational statements, of course, can be used to formulate finite element methods. A discretized version of (4.8) provides a finite element formulation for the fundamental eigenproblem, while (4.7) leads to the development of a traction-oriented finite element method that has some distinct advantages over existing approaches for the solution of general smooth and non-smooth boundary value problems.

By starting with (4.7), discretizing the domain and boundary, and interpolating weighted traction on the boundary, we obtain

$$\int_V \delta\boldsymbol{U}^{\mathrm{T}}\boldsymbol{B}^{\mathrm{T}}\boldsymbol{C}\boldsymbol{B}\boldsymbol{U}\,\mathrm{d}V = \int_S \delta\boldsymbol{U}^{\mathrm{T}}\boldsymbol{N}^{\mathrm{T}}\boldsymbol{\Phi}\boldsymbol{N}\boldsymbol{T}^{\varphi}\,\mathrm{d}S \tag{4.9}$$

where $\boldsymbol{C}$ represents the elastic constitutive tensor in matrix form and $\boldsymbol{B}$ is the usual matrix of shape function derivatives. Introducing $\boldsymbol{K}$ and $\boldsymbol{S}^{\varphi}$, this can be written

$$\delta\boldsymbol{U}^{\mathrm{T}}\boldsymbol{K}\boldsymbol{U} = \delta\boldsymbol{U}^{\mathrm{T}}\boldsymbol{S}^{\varphi}\boldsymbol{T}^{\varphi} \tag{4.10}$$

Finally, since $\delta\boldsymbol{U}^{\mathrm{T}}$ is arbitrary, we establish (4.6).

Partitioning the left-hand side of (4.6) to correspond with the right-hand side, we obtain

$$\begin{bmatrix} \boldsymbol{K}_{\mathrm{BB}} & \boldsymbol{K}_{\mathrm{BI}} \\ \boldsymbol{K}_{\mathrm{BB}}^{\mathrm{T}} & \boldsymbol{K}_{\mathrm{II}} \end{bmatrix} \begin{Bmatrix} \boldsymbol{U}_{\mathrm{B}} \\ \boldsymbol{U}_{\mathrm{I}} \end{Bmatrix} = \begin{Bmatrix} \boldsymbol{S}^{\varphi}\boldsymbol{T}^{\varphi} \\ \boldsymbol{0} \end{Bmatrix} \tag{4.11}$$

where $\boldsymbol{U}_{\mathrm{B}}$ and $\boldsymbol{U}_{\mathrm{I}}$ are the vectors of nodal displacement for boundary and interior nodes, respectively. From the second set of equations,

$$\boldsymbol{U}_{\mathrm{I}} = -\boldsymbol{K}_{\mathrm{II}}^{-1}\boldsymbol{K}_{\mathrm{BI}}^{\mathrm{T}}\boldsymbol{U}_{\mathrm{B}} \tag{4.12}$$

and therefore in terms of boundary nodes, we can write

$$\overline{\boldsymbol{K}}_{\mathrm{BB}}\boldsymbol{U}_{\mathrm{B}} = \boldsymbol{S}^{\varphi}\boldsymbol{T}^{\varphi} \tag{4.13}$$

where $\overline{\boldsymbol{K}}_{\mathrm{BB}}$ is the boundary stiffness matrix defined by

$$\overline{\boldsymbol{K}}_{\mathrm{BB}} = \boldsymbol{K}_{\mathrm{BB}} - \boldsymbol{K}_{\mathrm{BI}}\boldsymbol{K}_{\mathrm{II}}^{-1}\boldsymbol{K}_{\mathrm{BI}}^{\mathrm{T}} \tag{4.14}$$

Notice that the finite element formulation expressed in (4.13) is now the analog of the boundary element method presented in (3.4). In the boundary element formulation the volume integrals are transformed analytically to the boundary using the divergence theorem, whereas in this finite element method the transformation is performed numerically via condensation. It should be mentioned that $\boldsymbol{S}^{\varphi}$ can be a rectangular matrix, similar to $\boldsymbol{G}^{\varphi}$ in the boundary element method, to permit discontinuity in the weighted traction vector $\boldsymbol{T}^{\varphi}$. However, the character of $\boldsymbol{S}^{\varphi}$ is quite different from $\boldsymbol{G}^{\varphi}$, and this affects the relative performance of the two methods, particularly for non-smooth problems.

Notice that $\boldsymbol{S}^{\varphi}$ is a banded matrix in contrast to $\boldsymbol{G}^{\varphi}$ which is a full matrix. In practice it is customary to have new elements wherever the boundary condition changes. These properties enable us to solve first for unknown displacements in (4.6) or (4.13) and then solve for the unknown weighted tractions. The process for finding displacements is exactly like in the standard finite element with nodal forces and symmetric modified stiffness matrix. In other words the choice of $\varphi$ does not have any affect on displacements. In boundary element methods, this is not true. Unknowns are coupled and the choice of $\varphi$ does affect the displacements.

The corresponding generalized fundamental eigenproblem for the traction-oriented finite element method can also be formulated strictly in terms of boundary nodes and written as

$$\overline{\boldsymbol{K}}_{\mathrm{BB}}\boldsymbol{U}_{\mathrm{B}} = \lambda\widehat{\boldsymbol{S}}^{\varphi}\boldsymbol{U}_{\mathrm{B}} \tag{4.15}$$

The matrix $\overline{\boldsymbol{K}}_{\mathrm{BB}}$ is symmetric positive semi-definite. Assuming that the shape functions for traction are identical with those for displacements on the boundary, $\widehat{\boldsymbol{S}}^{\varphi}$ is also (square) symmetric positive definite. Consequently, the eigenproblem associated with this traction-oriented finite element method has real eigenvalues and eigenvectors, which are orthogonal with respect to $\overline{\boldsymbol{K}}_{\mathrm{BB}}$ and $\widehat{\boldsymbol{S}}^{\varphi}$

$$\boldsymbol{U}_{\mathrm{B}}^{(m)\mathrm{T}}\overline{\boldsymbol{K}}_{\mathrm{BB}}\boldsymbol{U}_{\mathrm{B}}^{(n)} = 0 \quad \text{for } m \neq n \tag{4.16}$$

$$\boldsymbol{U}_{\mathrm{B}}^{(m)\mathrm{T}}\widehat{\boldsymbol{S}}^{\varphi}\boldsymbol{U}_{\mathrm{B}}^{(n)} = 0 \quad \text{for } m \neq n \tag{4.17}$$

We have to keep in mind that the choice of $\varphi$ affects eigensolutions is general.

It should be mentioned that the eigenvectors $\boldsymbol{U}_{\mathrm{B}}^{(n)}$ are associated with only boundary nodes. By assuming orthonormality of eigenvectors with respect to $\widehat{\boldsymbol{S}}^{\varphi}$

$$\boldsymbol{U}_{\mathrm{B}}^{(m)\mathrm{T}}\widehat{\boldsymbol{S}}^{\varphi}\boldsymbol{U}_{\mathrm{B}}^{(m)} = 1 \quad m = 1, 2, \ldots, N \tag{4.18}$$

then

$$\boldsymbol{U}_{\mathrm{B}}^{(m)\mathrm{T}}\overline{\boldsymbol{K}}_{\mathrm{BB}}\boldsymbol{U}_{\mathrm{B}}^{(m)} = \lambda_m \quad m = 1, 2, \ldots, N \tag{4.19}$$

By defining the boundary modal matrix

$$\mathscr{U}_{\mathscr{B}} = [\boldsymbol{U}_{\mathrm{B}}^{(1)}\boldsymbol{U}_{\mathrm{B}}^{(2)}\cdots\boldsymbol{U}_{\mathrm{B}}^{(N)}] \tag{4.20}$$

where each column of the matrix is a normalized eigenvector, we have

$$\mathscr{U}_{\mathscr{B}}^{\mathrm{T}}\widehat{\boldsymbol{S}}^{\varphi}\boldsymbol{U}_{\mathrm{B}} = \boldsymbol{I} \tag{4.21}$$

$$\mathscr{U}_{\mathscr{B}}^{\mathrm{T}}\overline{\boldsymbol{K}}_{\mathrm{BB}}\boldsymbol{U}_{\mathrm{B}} = \boldsymbol{\Lambda} \tag{4.22}$$

where $\boldsymbol{I}$ is the unit matrix of order $N$ and $\boldsymbol{\Lambda}$ represents the diagonal matrix of the $N$ eigenvalues.

Solutions $\boldsymbol{U}_{\mathrm{B}}$ of (4.13) implicitly utilize the eigenvectors of (4.15) as a basis. For a problem with $d$ spatial dimensions and $N_{\mathrm{B}}$ boundary nodes, we have

$$\boldsymbol{U}_{\mathrm{B}} = \sum_{n=1}^{N}\tilde{A}_n\boldsymbol{U}_{\mathrm{B}}^{(n)} \tag{4.23}$$

where $N = dN_{\mathrm{B}}$ and

$$\tilde{A}_n = \boldsymbol{U}_{\mathrm{B}}^{\mathrm{T}}\widehat{\boldsymbol{S}}^{\varphi}\boldsymbol{U}_{\mathrm{B}}^{(n)} \tag{4.24}$$

Alternatively, this can be written

$$\tilde{\boldsymbol{u}} = \sum_{n=1}^{N}\tilde{A}_n\tilde{\boldsymbol{u}}^{(n)} \tag{4.25}$$

with

$$\tilde{A}_n = \int_S \varphi_{ij}u_i\tilde{u}_j^{(n)}\,\mathrm{d}S \quad n = 1, 2, \ldots, N \tag{4.26}$$

where $\tilde{\boldsymbol{u}}(x) = \boldsymbol{N}(x)\boldsymbol{U}_{\mathrm{B}}$ is the finite element solution on the boundary $S$ and $\tilde{\boldsymbol{u}}^{(n)}(x)$ are the approximated eigenmodes.

We note that for a Dirichlet problem (displacement prescribed boundary condition) the values of the approximated Fourier coefficients $\tilde{A}_n$ determined from (4.24) and (4.26) are identical, since $\tilde{\boldsymbol{u}}$ is then the

orthogonal projection of $\boldsymbol{u}$ onto the span $\{\tilde{\boldsymbol{u}}^{(1)}, \tilde{\boldsymbol{u}}^{(2)}, \ldots, \tilde{\boldsymbol{u}}^{(N)}\}$. For a Neumann problem (traction prescribed boundary condition)

$$\tilde{\boldsymbol{t}}^{\varphi} = \sum_{n=1}^{N} \tilde{A}_n \tilde{\lambda}_n \tilde{\boldsymbol{u}}^{(n)} \quad \text{on } S \tag{4.27}$$

with

$$\tilde{A}_n = \frac{1}{\tilde{\lambda}_n} \int_S t_i \tilde{u}_i^{(n)} \, \mathrm{d}S \quad n = n_{\mathrm{R}} + 1, \ldots, N \tag{4.28}$$

where $n_{\mathrm{R}}$ is the number of rigid body modes. Coefficients corresponding to $\lambda_n = 0$ are not determined, because we can add an arbitrary rigid body motion to the solution in the Neumann problem.

In general, we see that the solution is a linear combination of fundamental eigensolutions (or eigenmodes). The number of these eigenmodes in a discretized finite element model relates to the number of boundary nodes, not to the number of interior nodes. Interior nodes only help to improve the accuracy of the fundamental eigenmodes.

Let us look at the boundary stiffness matrix $\overline{\boldsymbol{K}}_{\mathrm{BB}}$ more carefully. First we see that the strain energy can be written in terms of boundary and interior nodes as follows:

$$\mathscr{U} = \tfrac{1}{2} \boldsymbol{U}^{\mathrm{T}} \boldsymbol{K} \boldsymbol{U} \tag{4.29}$$

By partitioning the right-hand side and using (4.12) for equilibrium

$$\mathscr{U} = \tfrac{1}{2} \boldsymbol{U}_{\mathrm{B}}^{\mathrm{T}} \overline{\boldsymbol{K}}_{\mathrm{BB}} \boldsymbol{U}_{\mathrm{B}} \tag{4.30}$$

which is the strain energy at equilibrium in terms of the boundary nodes only. Also from (4.21) and (4.22), we have

$$\overline{\boldsymbol{K}}_{\mathrm{BB}} = \widehat{\boldsymbol{S}}^{\varphi} \mathscr{U}_{\mathscr{B}} \boldsymbol{\Lambda} \mathscr{U}_{\mathscr{B}}^{\mathrm{T}} \widehat{\boldsymbol{S}}^{\varphi \mathrm{T}}$$

This is reminiscent of the following form of strain energy developed in Part I

$$\mathscr{U} = \int_S \oint\!\!\!\!\!\!= \int_S k_{ij}(x,y) u_j(y) u_i(x) \, \mathrm{d}S(x) \, \mathrm{d}S(y) \tag{4.31}$$

where $\boldsymbol{k}(x,y)$ is the hypersingular boundary stiffness kernel. After discretizing the boundary and using shape functions

$$\mathscr{U} = \tfrac{1}{2} \boldsymbol{U}_{\mathrm{B}}^{\mathrm{T}} \boldsymbol{K}_{\mathrm{bb}} \boldsymbol{U}_{\mathrm{B}} \tag{4.32}$$

where

$$\boldsymbol{K}_{\mathrm{bb}} = \int_S \oint\!\!\!\!\!\!= \int_S \boldsymbol{N}^{\mathrm{T}}(x) \boldsymbol{k}(x,y) \boldsymbol{N}(y) \, \mathrm{d}S(x) \, \mathrm{d}S(y) \tag{4.33}$$

We have to call $\boldsymbol{K}_{\mathrm{bb}}$ again the *boundary stiffness matrix*. It is seen that $\overline{\boldsymbol{K}}_{\mathrm{BB}}$ is a more approximated form of $\boldsymbol{K}_{\mathrm{bb}}$. While $\overline{\boldsymbol{K}}_{\mathrm{BB}}$ is derived from the virtual work theorem in the volume and then numerically condensed to the boundary nodes, $\boldsymbol{K}_{\mathrm{bb}}$ is obtained from the virtual work in the form of double surface integration. Although in general we do not have the hypersingular boundary stiffness kernel $\boldsymbol{k}(x,y)$ available, this formulation shows the deep relation of finite element methods with boundary integral equations. From now on, in principle, we can use either $\overline{\boldsymbol{K}}_{\mathrm{BB}}$ or $\boldsymbol{K}_{\mathrm{bb}}$.

Let us write the boundary integral version of the weak formulation

$$\int_S \oint\!\!\!\!\!\!= \int_S k_{ij}(x,y) u_j(y) \delta u_i(x) \, \mathrm{d}S(y) \, \mathrm{d}S(x) = \int_S t_i(x) \delta u_i(x) \, \mathrm{d}S(x) \tag{4.34}$$

or by using weighted traction with $\varphi_{ij} = \varphi\delta_{ij}$

$$\int_S \oint_S k_{ij}(x,y)u_j(y)\delta u_i(x)\,\mathrm{d}S(y)\,\mathrm{d}S(x) = \int_S \varphi(x)t_i^{\varphi}(x)\delta u_i(x)\,\mathrm{d}S(x) \tag{4.35}$$

After discretizing the *boundary*

$$\delta \boldsymbol{U}_{\mathrm{B}}^{\mathrm{T}}\boldsymbol{K}_{\mathrm{bb}}\boldsymbol{U}_{\mathrm{B}} = \delta \boldsymbol{U}_{\mathrm{B}}^{\mathrm{T}}\boldsymbol{S}^{\varphi}\boldsymbol{T}^{\varphi}$$

However, since $\delta \boldsymbol{U}_{\mathrm{B}}$ is arbitrary, we have

$$\boldsymbol{K}_{\mathrm{bb}}\boldsymbol{U}_{\mathrm{B}} = \boldsymbol{S}^{\varphi}\boldsymbol{T}^{\varphi} \tag{4.36}$$

The eigenvalue problem in terms of the boundary stiffness matrix can be written as

$$\boldsymbol{K}_{\mathrm{bb}}\boldsymbol{U}_{\mathrm{B}} = \lambda\widehat{\boldsymbol{S}}^{\varphi}\boldsymbol{U}_{\mathrm{B}} \tag{4.37}$$

Since rigid body motion does not generate any stresses, the matrix $\boldsymbol{K}_{\mathrm{bb}}$ is singular. This is obvious from theory of fundamental eigensolutions which includes rigid body eigenmodes corresponding to $\lambda = 0$.

We should emphasize again that the shape functions for weighted traction are assumed identical with those for displacements on the boundary. This is very important in the computational aspects. In this case, $\widehat{\boldsymbol{S}}^{\varphi}$ for the eigenproblem is a symmetric positive definite matrix which guarantees the reality and orthogonality of the eigensolutions.

It is possible to write the orthogonality with respect to the total stiffness matrix. From Part I, we recall

$$\int_V \sigma_{ij}^{(m)}\varepsilon_{ij}^{(n)}\,\mathrm{d}V = \begin{cases} 0 & \text{for } m \neq n \\ \lambda_m & \text{for } m = n \end{cases}$$

Then, in matrix form we obtain

$$\boldsymbol{U}^{(m)\mathrm{T}}\boldsymbol{K}\boldsymbol{U}^{(n)} = \begin{cases} 0 & \text{for } m \neq n \\ \lambda_m & \text{for } m = n \end{cases}$$

where $\boldsymbol{U}^{(m)}$ is the displacement vector over the entire domain associated with boundary eigenmode $m$.

By defining the rectangular global modal matrix

$$\mathscr{U} = [\boldsymbol{U}^{(1)}\boldsymbol{U}^{(2)}\cdots\boldsymbol{U}^{(N)}] \tag{4.38}$$

where each column of the matrix is an eigenvector normalized on the boundary, we have

$$\mathscr{U}^{\mathrm{T}}\boldsymbol{K}\boldsymbol{U} = \boldsymbol{\Lambda} \tag{4.39}$$

Finally, at the end of this discussion, it should be mentioned that eigensolutions of the total stiffness matrix in traditional finite element methods (e.g., Bathe, 1996)

$$\boldsymbol{K}\boldsymbol{V} = \rho\boldsymbol{V} \tag{4.40}$$

do not approximate the fundamental boundary eigensolutions. The eigensolutions $(\rho, \boldsymbol{V})$ of (4.40) are actually dynamic eigenmodes of the free body with unit lumped masses at all nodes, internal and boundary. Actually these dynamical eigenmodes provide an orthogonal basis for a particular solution due to body forces. Traditional finite element methods can approximate boundary eigensolutions if we consider lumped masses only at boundary nodes. For a uniform boundary discretization, this could be written

$$\begin{bmatrix} \boldsymbol{K}_{\mathrm{BB}} & \boldsymbol{K}_{\mathrm{BI}} \\ \boldsymbol{K}_{\mathrm{BI}}^{\mathrm{T}} & \boldsymbol{K}_{\mathrm{II}} \end{bmatrix}\begin{Bmatrix} \boldsymbol{V}_{\mathrm{B}} \\ \boldsymbol{V}_{\mathrm{I}} \end{Bmatrix} = \lambda'\begin{bmatrix} \boldsymbol{I} & \boldsymbol{0} \\ \boldsymbol{0} & \boldsymbol{0} \end{bmatrix}\begin{Bmatrix} \boldsymbol{V}_{\mathrm{B}} \\ \boldsymbol{V}_{\mathrm{I}} \end{Bmatrix} \tag{4.41a}$$

or

$$\overline{\boldsymbol{K}}_{\mathrm{BB}}\boldsymbol{V}_{\mathrm{B}} = \lambda'\boldsymbol{V}_{\mathrm{B}} \tag{4.41b}$$

### 4.2. Convergence analysis

We showed in Section 2 that the theory of fundamental eigenexpansion provides both global and local convergence criteria. As mentioned above, the eigensolutions of the traction-oriented finite element formulation yield approximations of the lowest eigensolutions of the fundamental problem. The infinite series and partial sum eigenexpansions are presented in (2.3) and (2.7), respectively. We will now show that under certain circumstances the finite element solutions of (4.13) represented by (4.23) or (4.25), where even the eigenmodes are approximated, converge in the mean to $\boldsymbol{u}$. This is accomplished by first demonstrating that the values of $\tilde{A}_n$ from (4.26) minimize the error norm $\|\boldsymbol{u}-\tilde{\boldsymbol{u}}\|$ where

$$\|\boldsymbol{u}-\tilde{\boldsymbol{u}}\|^2 = \int_S \varphi_{ij}(u_i-\tilde{u}_i)(u_j-\tilde{u}_j)\,\mathrm{d}S \tag{4.42}$$

We assume in the following that both exact and approximated eigenmodes have been orthonormalized.

Expanding (4.42) provides

$$\|\boldsymbol{u}-\tilde{\boldsymbol{u}}\|^2 = \int_S \varphi_{ij}u_iu_j\,\mathrm{d}S + \int_S \varphi_{ij}\tilde{u}_i\tilde{u}_j\,\mathrm{d}S - 2\int_S \varphi_{ij}u_i\tilde{u}_j\,\mathrm{d}S \tag{4.43}$$

Then after substituting (2.3) and (4.25) into (4.43) and invoking the orthonormality conditions, we obtain

$$\|\boldsymbol{u}-\tilde{\boldsymbol{u}}\|^2 = \sum_{n=1}^{\infty} A_n^2 + \sum_{n=1}^{N}\tilde{A}_n^2 - 2\sum_{n=1}^{N}\tilde{A}_n\int_S \varphi_{ij}u_i\tilde{u}_j^{(n)}\,\mathrm{d}S \tag{4.44}$$

For a minimum, we must have

$$\frac{\partial}{\partial\tilde{A}_m}\|\boldsymbol{u}-\tilde{\boldsymbol{u}}\|^2 = 0 \quad \text{for } m=1,2,\ldots,N$$

Then

$$\tilde{A}_m = \int_S \varphi_{ij}u_i\tilde{u}_j^{(m)}\,\mathrm{d}S \quad m=1,2,\ldots,N \tag{4.45}$$

This agrees with (4.26).

Substituting (4.45) into (4.44), we obtain for the minimum value of the norm

$$\|\boldsymbol{u}-\tilde{\boldsymbol{u}}\|^2_{\min} = \sum_{n=1}^{\infty} A_n^2 + \sum_{n=1}^{N}\tilde{A}_n^2 - 2\sum_{n=1}^{N}\tilde{A}_n^2$$

and finally

$$\|\boldsymbol{u}-\tilde{\boldsymbol{u}}\|_{\min} = \left[\sum_{n=1}^{\infty} A_n^2 - \sum_{n=1}^{N}\tilde{A}_n^2\right]^{\frac{1}{2}} \tag{4.46}$$

We can also show that the Fourier coefficient (4.28) minimizes the error norm $\|\boldsymbol{t}^{\varphi}-\tilde{\boldsymbol{t}}^{\varphi}\|$ where

$$\|\boldsymbol{t}^{\varphi}-\tilde{\boldsymbol{t}}^{\varphi}\|^2 = \int_S \varphi_{ij}(t_i^{\varphi}-\tilde{t}_i^{\varphi})(t_j^{\varphi}-\tilde{t}_j^{\varphi})\,\mathrm{d}S \tag{4.47}$$

By expanding (4.47)

$$\|\boldsymbol{t}^{\varphi}-\tilde{\boldsymbol{t}}^{\varphi}\|^2 = \int_S \varphi_{ij}t_i^{\varphi}t_j^{\varphi}\,\mathrm{d}S + \int_S \varphi_{ij}\tilde{t}_i^{\varphi}\tilde{t}_j^{\varphi}\,\mathrm{d}S - 2\int_S \varphi_{ij}\tilde{t}_i^{\varphi}t_j^{\varphi}\,\mathrm{d}S$$

or

$$\|\boldsymbol{t}^{\varphi} - \tilde{\boldsymbol{t}}^{\varphi}\|^2 = \sum_{n=1}^{\infty} \lambda_n^2 A_n^2 + \sum_{n=1}^{N} \tilde{\lambda}_n^2 \tilde{A}_n^2 - 2 \sum_{n=1}^{N} \tilde{\lambda}_n \tilde{A}_n \int_S t_i \tilde{u}_i^{(n)} \, \mathrm{d}S$$

Then for a minimum,

$$2\tilde{\lambda}_m^2 \tilde{A}_m - 2\tilde{\lambda}_m \int_S t_i \tilde{u}_i^{(m)} \, \mathrm{d}S = 0 \quad m = 1, 2, \ldots, N$$

Keeping in mind the indeterminacy of Fourier coefficients for rigid body modes in the Neumann problem, we have

$$\tilde{\lambda}_m \tilde{A}_m = \int_S t_i \tilde{u}_j^{(m)} \, \mathrm{d}S \quad m = 1, 2, 3, \ldots, N \tag{4.48}$$

which agrees with (4.28). The corresponding minimum value is

$$\|\boldsymbol{t}^{\varphi} - \tilde{\boldsymbol{t}}^{\varphi}\|_{\min} = \left[ \sum_{n=1}^{\infty} \lambda_n^2 A_n^2 - \sum_{n=1}^{N} \tilde{\lambda}_n^2 \tilde{A}_n^2 \right]^{\frac{1}{2}} \tag{4.49}$$

It should be emphasized that the quantities inside the brackets on the right-hand side of (4.46) and (4.49) are non-negative.

The question remains, are the finite element solutions $\boldsymbol{U}_{\mathrm{B}}$ and $\boldsymbol{T}^{\varphi}$ obtained from (4.13) consistent with the approximate solutions $\tilde{\boldsymbol{u}}$ and $\tilde{\boldsymbol{t}}^{\varphi}$ determined from these finite partial eigenexpansions? For the Dirichlet problem, the two solutions are consistent. If identical rigid body motions are selected for the exact and approximated displacement field in the Neumann problem with continuous tractions, then again the two solutions are consistent. Thus, in these cases, the displacement and weighted traction error norms are minimum for the traction-oriented finite element solution. However, this is not the case for mixed problems. The finite element solution, based upon (4.13), employs a rectangular form of $\boldsymbol{S}^{\varphi}$ and uses a combination of components from $\boldsymbol{U}_{\mathrm{B}}$ and $\boldsymbol{T}^{\varphi}$ as unknowns. Consequently, the finite element displacement and weighted traction error norms do not, in general, assume a minimum value.

### *4.3. Numerical implementation*

The numerical implementation of the traction-oriented finite element method is quite straightforward. Any standard finite element code can be used to condense the global stiffness matrix to the boundary nodes. In our work, the frontal solver in the geotechnical program CRISP (Gunn and Britto, 1984) was modified to provide $\overline{\boldsymbol{K}}_{\mathrm{BB}}$. Meanwhile the boundary matrix $\boldsymbol{S}^{\varphi}$ (or $\widehat{\boldsymbol{S}}^{\varphi}$) is evaluated using gaussian quadrature. In some cases, the integrand in $\boldsymbol{S}^{\varphi}$ is weakly singular at the non-smooth points. Transformations can be introduced to permit exact integration or numerical quadrature following standard boundary element concepts can be employed.

Once the two matrices $\overline{\boldsymbol{K}}_{\mathrm{BB}}$ and $\widehat{\boldsymbol{S}}^{\varphi}$ are established, the fundamental eigenproblem defined in (4.15) can be solved using the symmetric generalized eigensolvers available in the LAPACK package (Anderson et al., 1992). All of the eigenvalues and eigenvectors are real valued.

However, we re-emphasize that for the direct solution of boundary value problems, we do not need to solve the eigenproblem. Instead, we can work directly with (4.6) or (4.13). Standard boundary element assembly and solution methodology can be utilized to solve that system. In some non-smooth problems,

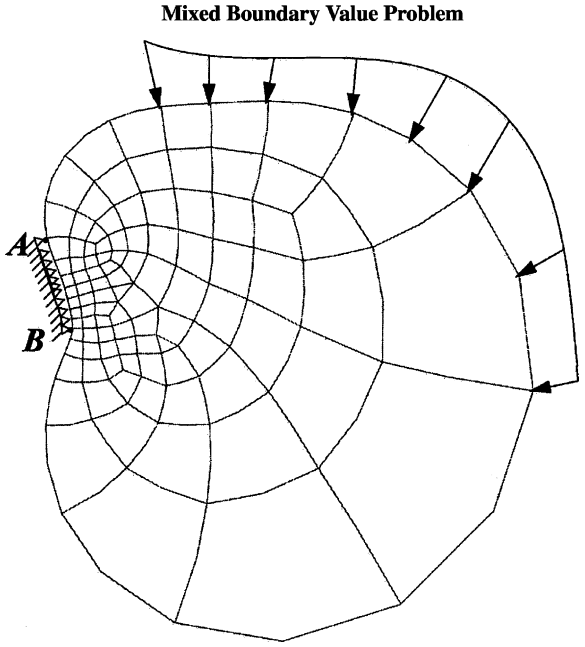


Fig. 1. Mixed boundary value problem—problem definition.

such as those involving bi-material interfaces, a multi-region approach may be adopted (e.g., Banerjee, 1994). Although this is non-standard within the context of finite element methods, it provides a methodology that is consistent with the theory of boundary value problems. Furthermore, it should be clear that we need not actually form the boundary stiffness matrix $\overline{\boldsymbol{K}}_{\mathrm{BB}}$. This was done only to emphasize the connection with the theory of the fundamental eigenproblem and boundary element methods. In practice, we can work directly with (4.6). For certain representations of $\boldsymbol{T}^{\varphi}$, the formulation can be further simplified.

Consider the generic finite element discretization of a mixed boundary value problem, shown in Fig. 1. The specified boundary conditions lead to a partitioning of boundary displacements and weighted tractions as follows:

$$\boldsymbol{U}_{\mathrm{B}} = \left\{ \begin{array}{c} \boldsymbol{U}_t \\ \boldsymbol{U}_u \end{array} \right\}, \quad \boldsymbol{T}^{\varphi} = \left\{ \begin{array}{c} \boldsymbol{T}^{\varphi}_t \\ \boldsymbol{T}^{\varphi}_u \end{array} \right\} \tag{4.50a, b}$$

where $\boldsymbol{U}_u$ and $\boldsymbol{T}^{\varphi}_t$ are known. Then, assuming nodal-based displacements and element-based weighted tractions, (4.13) can be written as

$$\left[ \begin{array}{cc} \overline{\boldsymbol{K}}_{tt} & \overline{\boldsymbol{K}}_{tu} \\ \overline{\boldsymbol{K}}_{ut} & \overline{\boldsymbol{K}}_{uu} \end{array} \right] \left\{ \begin{array}{c} \boldsymbol{U}_t \\ \boldsymbol{U}_u \end{array} \right\} = \left[ \begin{array}{cc} \boldsymbol{S}^{\varphi}_{tt} & \boldsymbol{0} \\ \boldsymbol{0} & \boldsymbol{S}^{\varphi}_{uu} \end{array} \right] \left\{ \begin{array}{c} \boldsymbol{T}^{\varphi}_t \\ \boldsymbol{T}^{\varphi}_u \end{array} \right\} \tag{4.51}$$

The zero off-diagonal blocks result from the use of piecewise continuous weighted traction elements having element edges coincident with all mixed boundary condition locations (i.e., points $A$ and $B$ in Fig. 1). After rearranging known and unknown solution variables, (4.51) becomes

$$\left[ \begin{array}{cc} \overline{\boldsymbol{K}}_{tt} & \boldsymbol{0} \\ \overline{\boldsymbol{K}}_{ut} & -\widehat{\boldsymbol{S}}^{\varphi}_{uu} \end{array} \right] \left\{ \begin{array}{c} \boldsymbol{U}_t \\ \widehat{\boldsymbol{T}}^{\varphi}_u \end{array} \right\} = \left\{ \begin{array}{c} \boldsymbol{F}_t \\ \boldsymbol{F}_u \end{array} \right\} \tag{4.52}$$

where $\widehat{\boldsymbol{T}}_u^{\varphi}$ represents the unknown weighted tractions that have now been assembled on a nodal basis, $\widehat{\boldsymbol{S}}_{uu}^{\varphi}$ is the corresponding square weighted boundary matrix, and the known right-hand side vector is determined from

$$\left\{ \begin{array}{c} \boldsymbol{F}_t \\ \boldsymbol{F}_u \end{array} \right\} = \left[ \begin{array}{cc} \boldsymbol{S}_{tt}^{\varphi} & -\overline{\boldsymbol{K}}_{tu} \\ \boldsymbol{0} & -\overline{\boldsymbol{K}}_{uu} \end{array} \right] \left\{ \begin{array}{c} \boldsymbol{T}_t^{\varphi} \\ \boldsymbol{U}_u \end{array} \right\} \tag{4.53}$$

Equation (4.52) indicates that the unknown nodal displacements can be found as an independent first step:

$$\overline{\boldsymbol{K}}_{tt} \boldsymbol{U}_t = \boldsymbol{F}_t \tag{4.54}$$

Interior displacements are then determined from (4.50a) and (4.12). This is exactly the traditional finite element elastostatic displacement solution and is unaffected by the choice of $\boldsymbol{\Phi}$. However, now weighted boundary tractions can be evaluated by solving

$$\widehat{\boldsymbol{S}}_{uu}^{\varphi} \widehat{\boldsymbol{T}}_u^{\varphi} = -\boldsymbol{F}_u + \overline{\boldsymbol{K}}_{ut} \boldsymbol{U}_t \tag{4.55}$$

Knowledge of $\boldsymbol{U}_{\mathrm{B}}$ and $\boldsymbol{T}^{\varphi}$ permits the direct evaluation of surface stresses. For smooth problems, this can be accomplished using the boundary element surface stress calculation algorithm (Cruse and Van Buren, 1971; Banerjee, 1994). Since there is no extrapolation involved, this approach is expected to produce more accurate boundary stresses than the standard procedures. Of course surface stresses are often of prime importance in elastostatic analyses.

Finally we should note that body forces can be handled in the usual manner. Thus (4.6) is extended to the form

$$\boldsymbol{K}\boldsymbol{U} = \left\{ \begin{array}{c} \boldsymbol{S}^{\varphi} \boldsymbol{T}^{\varphi} \\ \boldsymbol{0} \end{array} \right\} + \boldsymbol{P} \tag{4.56}$$

where $\boldsymbol{P}$ is a vector of nodal forces obtained via domain integration as in traditional finite element methods. However, here $\boldsymbol{P}$ excludes all contributions from the boundary traction.

## 5. Numerical examples

### 5.1. Introduction

In this section, we consider several numerical examples in order to study the performance of the new computational methods. First the fundamental eigenproblem is examined for a circle with unit radius under plane strain conditions. This represents a spectral analysis of the direct boundary element method and the traction-oriented finite element method. Results of both are compared with the analytical solution presented in Part I.

Then the emphasis shifts to the solution of boundary value problems. Stress analysis of a square plate with a central hole is the next example, which is categorized as a smooth problem. Afterwards, we direct our attention to the solution of non-smooth elastic boundary value problems. The examples include problems with mixed boundary conditions, an edge notch, an edge crack and a bi-material interface. In all of these examples, we solve the boundary value problem directly without explicitly determining the underlying generalized fundamental modes. We have employed (3.4) for the boundary element solutions and (4.13) for the finite element method. However, the theory of boundary eigensolutions is used to guide the development of the non-smooth boundary element and finite element formulations. Additionally the theory provides information concerning the quality of the numerical results. For example, if the weight function is properly selected, bounded values of the displacement and the weighted traction should result.

### 5.2. Elastostatic problem for unit circular disc

Consider an elastic circular disc with radius $a = 1$. Here we generate the fundamental eigenmodes for the plane strain case with $E = 1$ and $v = 0.3$, assuming $\varphi = 1$ on the boundary. Both traction-oriented finite element and boundary element methods are investigated by solving (4.15) and (3.7), respectively.

Three different meshes $A$, $B$ and $C$ have been used for the finite element analysis. In all cases, the elements are quadratic quadrilaterals. The number of nodes on the boundary is fixed at 96, thus forming 48 quadratic boundary elements. Table 1 shows some characteristics of the finite element meshes. The boundary element mesh consists of the same 48 quadratic boundary elements.

The finite element model for mesh $B$ is shown in Fig. 2. As we said the number of nodes on the boundary multiplied by the number of degrees-of-freedom per node gives the number of eigenmodes or degrees-of-freedom in the new concept. For both methods we have 192 eigensolutions. Increasing the number of internal nodes in the FEM meshes does not increase the number of eigenmodes. In other words, the number of degrees-of-freedom for both FEM and BEM methods is 192.

The LAPACK algorithm that was employed for the analysis extracts all of the eigenvalues. As noted previously, due to the lack of symmetry in the $\boldsymbol{F}$ and $\widehat{\boldsymbol{G}}$ matrices, the boundary element eigenproblem which approximates the real exact eigensolutions, can produce complex eigenvalues. In this particular example, two pairs of complex eigenvalues were found using double precision accuracy. However in all cases the imaginary part was less than $10^{-9}$ of the corresponding real part of the eigenvalue. The eigenvalues

Table 1
Finite element meshes for unit disc

| Mesh | Elements | Nodes |
|---|---|---|
| A | 104 | 361 |
| B | 432 | 1345 |
| C | 1008 | 3073 |

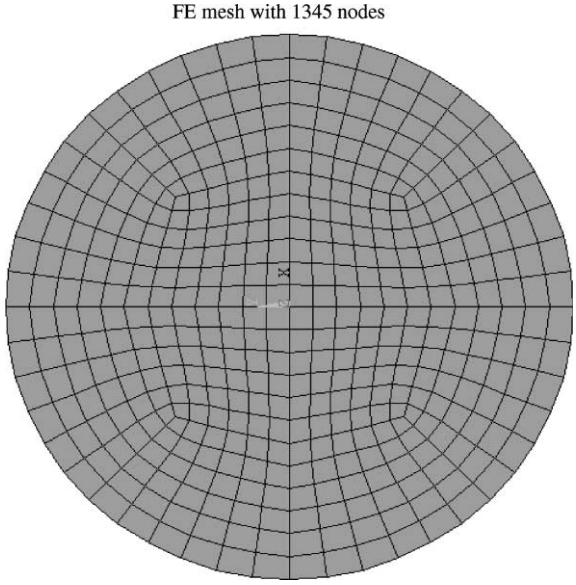


Fig. 2. Unit circular disc—finite element mesh B.

Table 2
Boundary eigenvalues for unit disc

| Mode | Type | Exact | BE | FE mesh A | FE mesh B | FE mesh C |
|---|---|---|---|---|---|---|
| 4 | I | 0.76923 | 0.76923 | 0.76924 | 0.76933 | 0.76955 |
| 8 | II | 1.2821 | 1.2821 | 1.2825 | 1.2821 | 1.2819 |
| 14 | III | 1.9231 | 1.9231 | 1.9231 | 1.9232 | 1.9235 |
| 15 | II | 2.1368 | 2.1376 | 2.1446 | 2.1370 | 2.1369 |
| 23 | I | 3.0769 | 3.0769 | 3.0781 | 3.0770 | 3.0771 |
| 25 | II | 3.4188 | 3.4263 | 3.5139 | 3.4237 | 3.4205 |
| 40 | I | 5.3846 | 5.3853 | 5.6025 | 5.3867 | 5.3864 |
| 60 | II | 8.1197 | 8.4676 | 9.4154 | 8.4859 | 8.3647 |
| 61 | I | 8.4615 | 8.4895 | 9.6632 | 8.8270 | 8.4805 |
| 80 | I | 10.769 | 11.532 | 14.158 | 12.084 | 11.631 |
| 81 | II | 11.111 | 11.877 | 14.378 | 12.300 | 11.631 |
| 100 | II | 13.675 | 16.637 | 21.444 | 19.845 | 16.459 |
| 150 | II | 20.513 | 27.914 | 66.293 | 47.074 | 34.445 |
| 190 | II | 26.069 | 34.581 | 287.82 | 126.47 | 63.033 |

obtained for some eigenmodes are listed in Table 2. The closed-form non-zero eigenvalues are type I equivoluminal modes for which

$$\lambda_m = \frac{2\tilde{\mu}m}{a} \quad m = 1, 2, \ldots$$

with a degeneracy of two, and type II eigenvalues

$$\lambda_m = \frac{2\tilde{\mu}m}{\kappa a} \quad m = 2, 3, \ldots$$

with a degeneracy of two in which $\kappa = 3 - 4\nu$. There is also a single eigenvalue (type III) corresponding to linear radial deformation

$$\lambda = \frac{4\tilde{\mu}}{(\kappa - 1)a} = \frac{2\tilde{\mu}}{(1 - 2\nu)a}$$

The closed-form expressions for all these eigenmodes are presented in Part I. In preparing Table 2, no attempt was made to correlate mode shapes. The entries for Mode 60, for example, are simply the sixtieth lowest eigenvalues obtained from the various analyses. It is seen that for lower modes, FEM has reasonably good eigenvalues similar to those of BEM. For higher modes, the eigenvalues in FEM become less accurate. However, increasing the number of internal nodes in FEM improves the eigenvalues and eigenmodes toward those obtained via BEM and the analytic ones (in Part I). This clearly shows why BEM can often solve problems more accurately for a given boundary discretization. In practice for FEM we usually increase internal and external nodes together. In this way with an FEM approach we increase the number of eigenmodes and improve the lowest ones. In general, we can also observe that the BEM and FEM generate more accurate equivoluminal eigensolutions (type I).

The BEM results for eigenmode 25 are shown in Fig. 3, along with FEM results of mesh $A$ and $C$ for this eigenmode. The result for even a very coarse internal mesh corresponding to mesh $A$ is quite similar to the result of BEM. Figure 4 shows the corresponding results for Mode 60. Now the result of the very coarse FEM internal mesh $A$ is far from the BEM results. By increasing the internal mesh, the mode gets improved toward the BEM result as is seen for mesh $C$ in Fig. 4. A detailed examination reveals that equivoluminal type I modes are captured much more accurately than type II modes with either numerical approach. As a result, some reordering of modes occurs. For example, all of the mode shapes shown in Fig. 4 are actually of type I and the mesh $A$ results correspond to a higher value of $m$.

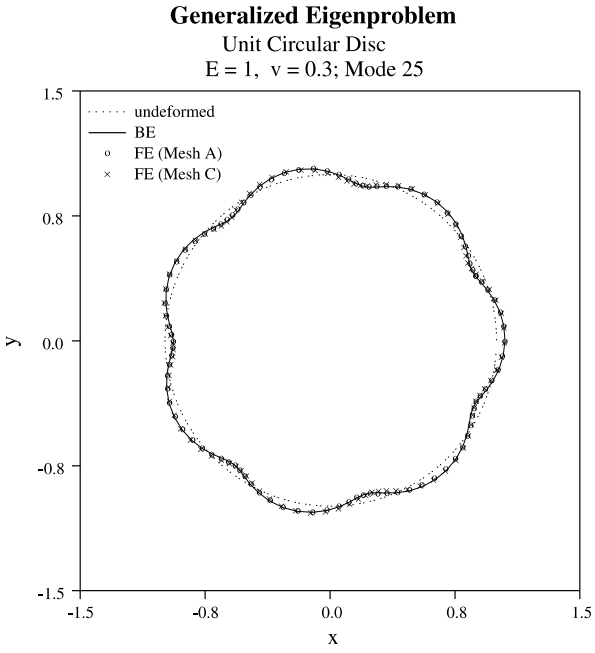


Fig. 3. Unit circular disc—eigenmodes for Mode 25.

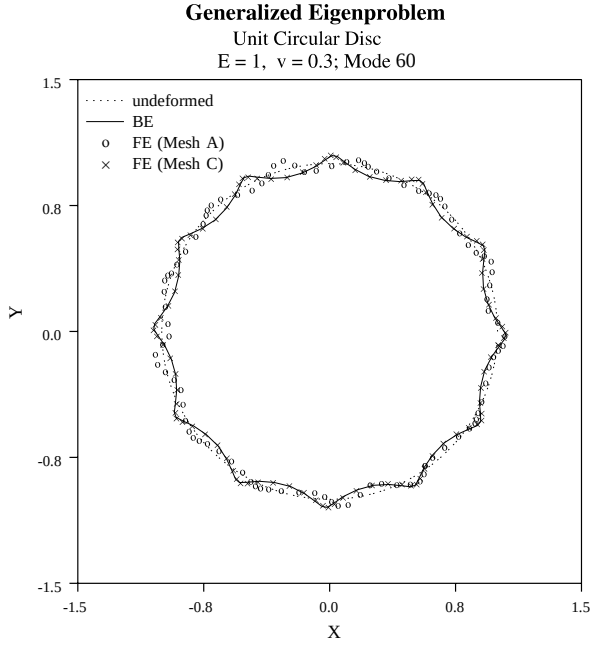


Fig. 4. Unit circular disc—eigenmodes for Mode 60.

Now consider a Dirichlet problem with the displacement on the unit circle prescribed as

$$u_x = \frac{xe^x}{2(1.1 + y^2)}$$

$$u_y = -\frac{ye^y}{2(1.1 + x^2)}$$

By using the discrete theory of fundamental eigenexpansion, the deformation can be written as

$$\widetilde{\boldsymbol{U}} = \sum_{n=1}^{N} \widetilde{\boldsymbol{A}}_n \widetilde{\boldsymbol{U}}_n$$

In the above mentioned FEM results, $N = 192$. The prescribed and reconstructed deformations obtained by Fourier analysis are shown in Fig. 5a using mesh $B$. There is good agreement between the two deformations. Figure 5b shows the spectrum of the Fourier coefficients.

Although, the boundary eigensolutions can be determined numerically from (3.7) or (4.15) and then used in a generalized Fourier analysis to solve boundary value problems, we do not advocate that approach since, in general, it is too expensive computationally. Instead, for the solution of boundary value problems, we only use the knowledge of the existence of these eigensolutions that underlie our solutions. In all of the following examples, we directly solve the boundary value problems using either (3.4) for boundary elements or (4.13) for finite elements. The simplifications detailed in Section 4.3 could also be invoked in the FEM analyses.

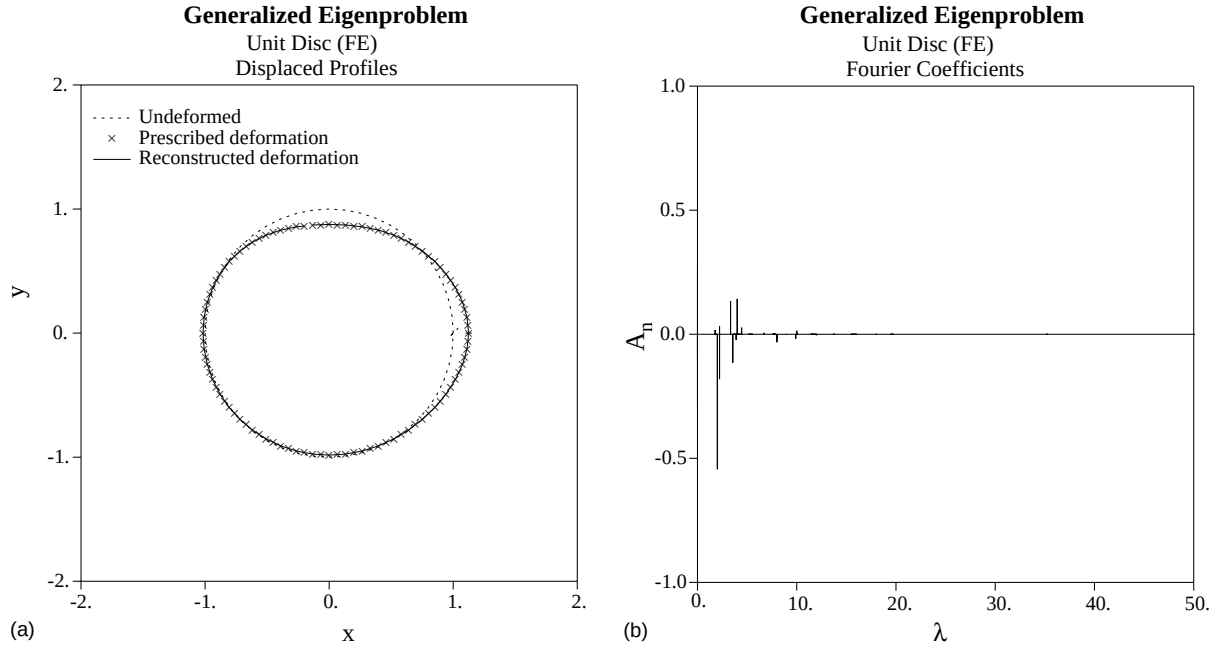


Fig. 5. Unit circular disc—spectrum analysis.

### 5.3. Stress analysis of a square plate with a circular hole

Next we use a standard boundary element method and the traction-oriented finite element method with $\varphi = 1$ to find the stress concentration in a square plate with a central hole as shown in Fig. 6. Plane strain conditions are assumed, with $E = 1$, $v = 0.3$ and traction $t_0 = 1$. We take $L = 1$ and $R = 0.4$. Due to symmetry in geometry and loading, only a quarter of the plate is considered. Three different levels of mesh refinement have been used, with the mesh characteristics presented in Table 3. Linear elements are used for representing the geometry of the models in both FEM and BEM, while for field quantities, quadratic elements are employed.

The results obtained for maximum nodal traction $t_x$ are presented in Table 4. Also listed in this table are the results from a doubly connected full body BEM analysis. With mesh refinement, the traction-oriented FEM produces peak stresses that are comparable to those obtained with the BEM approaches. A more detailed comparison of the traction distribution is provided in Fig. 7. Of course, in traditional FEM instead of nodal tractions, we have nodal forces. Therefore, nodal stresses are generally computed from extrapolation of gauss point stresses. In the traction-oriented finite element method, the surface tractions are evaluated directly as primary variables without extrapolation. Additionally, we can attempt to account for singularity by using an appropriate $\varphi$ as shown in the following examples.

### 5.4. Tension of a restrained rectangular plate

Let us now look at an apparently elementary problem in solid mechanics involving tension of a restrained rectangular plate as shown in Fig. 8. Boundary element solutions are obtained for $a = 3$ and $b = 1$. For this problem, an isotropic material in plane strain condition is assumed with $E = 1$. and $v = 0.3$. The left side of the plate is completely fixed. This not only makes the normal traction at the corners of the fixed side to be singular, but also generates a singular shear at these corners.

By introducing a proper weighting function, the boundary value problem can be solved completely in terms of bounded quantities. Since there are actually two singular points, the weighting function is chosen as the product $\varphi = r_1^{\gamma-1} r_2^{\gamma-1}$ where $r_1$ and $r_2$ are the radial distances defined in Fig. 8. This weight function is used on the left side of the plate and on the rest of the boundary we take $\varphi = 1$. From the analytical expansion of Williams (1952) for a free-fixed right angle wedge, one finds $\gamma \approx 0.7112$. Non-traditional shape

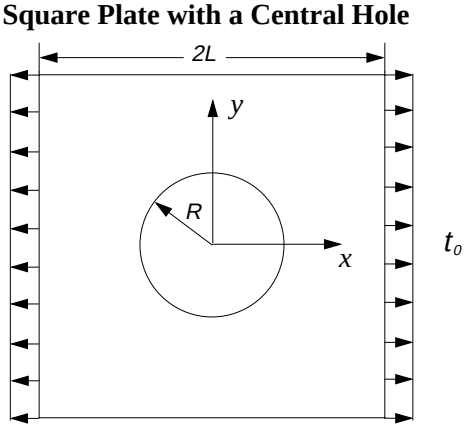


Fig. 6. Plate with circular hole—problem definition.

Table 3
Character of FE and BE meshes A, B and C for plate with circular hole

| Mesh | Number of finite elements | Number of nodes in FE model | Number of boundary elements | Number of nodes in BE model | Number of degrees of freedom |
|---|---|---|---|---|---|
| A | 48 | 173 | 28 | 56 | 112 |
| B | 140 | 469 | 48 | 96 | 192 |
| C | 560 | 1777 | 96 | 192 | 384 |

Table 4
Results for traction $t_x$ from different FE meshes for plate with circular hole

| Mesh | Traction-oriented FEM stress $t_x$ | Standard BEM stress $t_x$ | Standard BEM stress $t_x$ total body |
|---|---|---|---|
| A | 5.1588 | 5.1577 | 4.8071 |
| B | 4.9806 | 4.9867 | 4.7981 |
| C | 4.8287 | 4.8822 | 4.7902 |

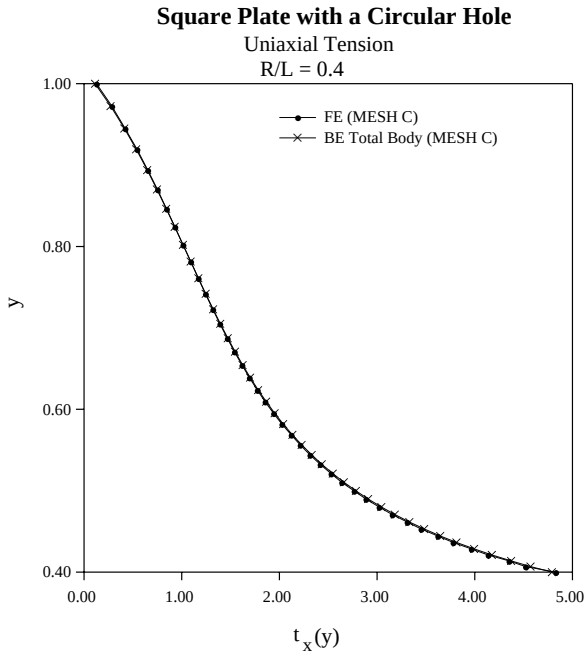


Fig. 7. Plate with circular hole—numerical solutions.

functions are also used for the displacement variation in elements immediately adjacent to the singular corners.

The problem is analyzed with our boundary element formulations and two levels of mesh refinement are examined. The coarse mesh employs 42 quadratic elements along the boundary shown in Fig. 8, while the refined model uses 84 elements. This corresponds to 168 and 336 boundary degrees-of-freedom, respectively.

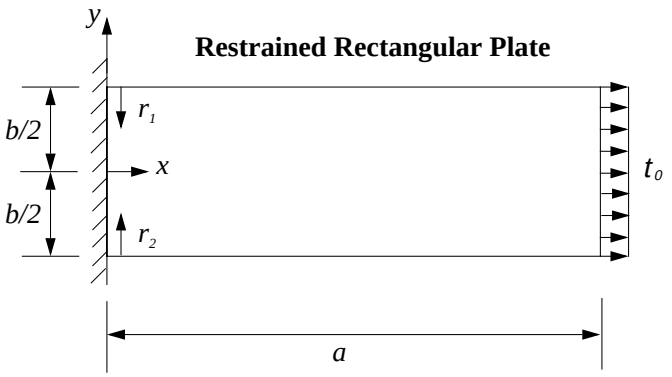


Fig. 8. Restrained rectangular plate—problem definition.

Boundary element results are presented in Fig. 9a. Nodal values of the weighted tractions $t_x^\varphi$ and $t_y^\varphi$ for the fine mesh are plotted versus distance along the left hand fixed edge. The results have converged away from the corners. Near the corners, there is a complicated variation of weighted traction. Significant mesh refinement is needed to capture $\boldsymbol{t}^\varphi$ on the fixed edge near the corner, and the associated singular and near-singular integrals must be evaluated accurately. The calculated behavior of $t_x^\varphi$ near the upper corner is shown in Fig. 9b for several levels of mesh refinement. The values of $t_x^\varphi$ and $t_y^\varphi$ at $y = (b/2)$ converge to $-0.441$ and 0.133, respectively.

By using $t_x = \varphi t_x^\varphi$ the distribution of traction $t_x$ can be determined. For the present non-smooth BEM, this produces the distribution shown in Fig. 9c, along with an infinite value at the corner. The result for $t_x$ from a standard boundary element analysis is also displayed in the figure. The standard BEM tractions exhibit significant oscillations and produce finite mesh-dependent values at the corner. On the other hand, the proposed non-smooth BEM formulation produces meaningful, mesh-independent solutions.

### 5.5. Plate with edge notch

Stress analysis of bodies with notches have not been extensively considered in the computational methods developed by engineers. We now apply the new boundary element and finite element methods for plane strain loading of a plate with an edge $V$-notch. Here we consider the geometry and boundary conditions shown in Fig. 10. Let $h = 5$, $w = 5$, $a = 1$ and $t_0 = 1$, while $2\alpha = 270°$ where $\alpha$ is the included half-angle at the notch. Material properties are $E = 1$ and $\nu = 0.3$. For stress analysis at the notch tip we can use a multi-region method, but here we use half-symmetry and model only the upper portion of the plate. As we mentioned, from the asymptotic expansion of Williams we know the singularity of stresses for free-free edges is $r^{\gamma-1}$ where $\gamma \approx 0.5445$ (Williams, 1952). Then the weight function

$$\varphi = \frac{1}{r^{1-\gamma}}$$

is used on the cut line. On the rest of the boundary, we take $\varphi = 1$.

In the numerical analysis, a coarse mesh with 200 degrees-of-freedom and a refined mesh with exactly twice as many boundary nodes are employed. In both cases, quadratic boundary elements are used. Meanwhile, the finite element domain models for the coarse and refined representations consist of 150 and 600 eight-noded quadratic elements, respectively.

Figure 11a and b provide the numerical solutions for the weighted traction $t_y^\varphi$ versus horizontal distance from the tip of the notch. Solutions away from the tip are converged. However, significant oscillations are

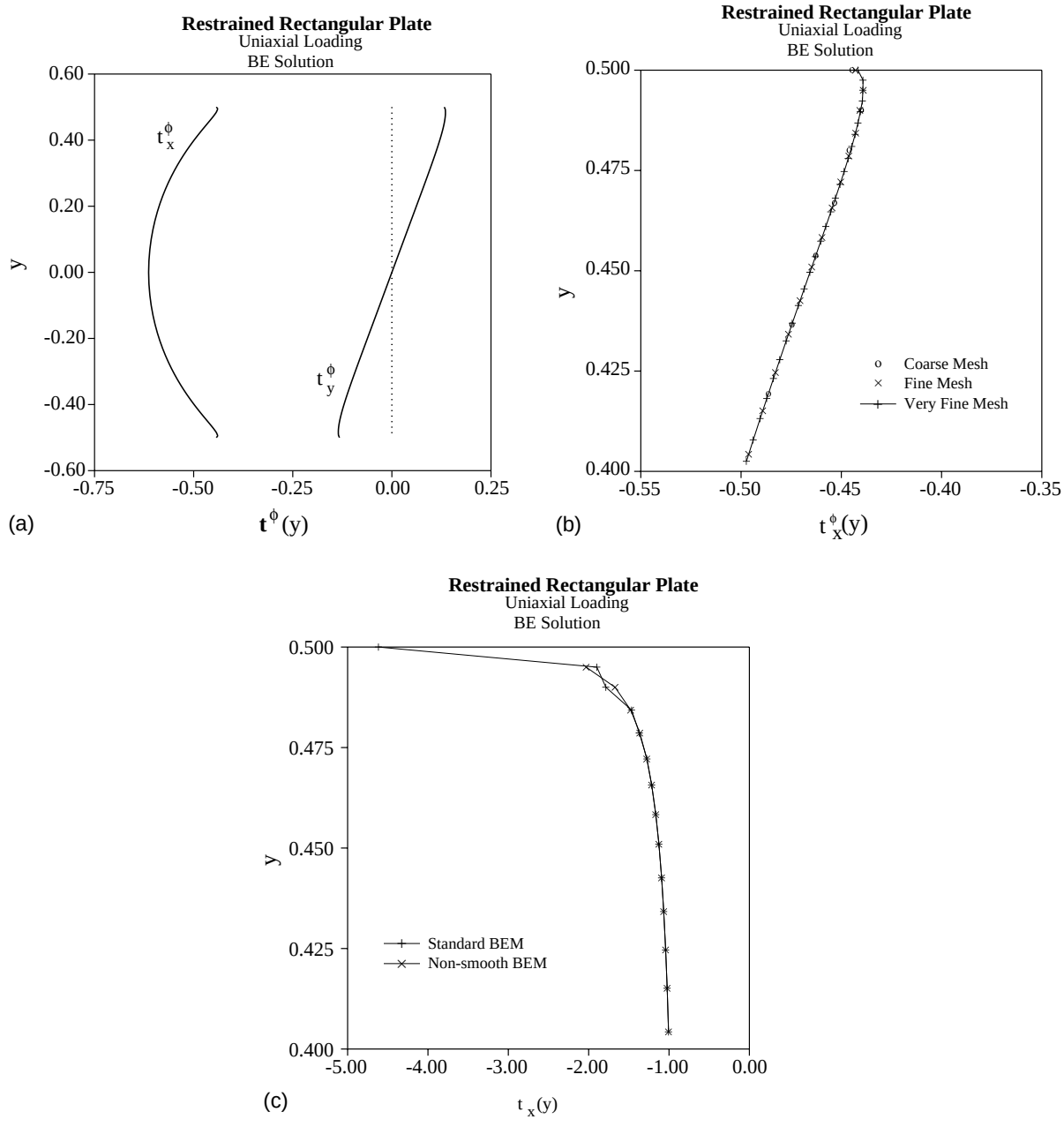


Fig. 9. Restrained rectangular plate—numerical solutions.

clearly visible in the vicinity of the notch in the FEM solutions. With increased mesh refinement the period of oscillations decreases but the amplitude remains consistent. The boundary element solutions do not exhibit oscillatory behavior. This can be attributed to the improved resolution of the higher fundamental eigenmodes obtained with the BEM formulation. Discontinuity induces participation from higher modes, and thus requires better accuracy of those modes to resolve the boundary variable.

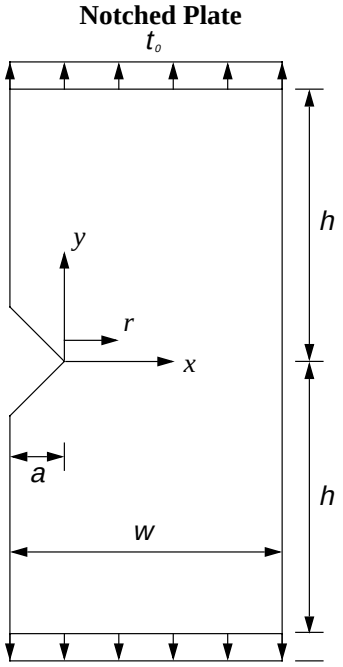


Fig. 10. Edge notch—problem definition.

We should emphasize that in the FEM formulation utilized here, the traction, or in this case weighted traction $\boldsymbol{t}^{\varphi}$, is a primary variable that is interpolated to the same level as the displacement $\boldsymbol{u}$. The traction component $t_y^{\varphi}$ at the tip is related to the general stress intensity factor $K_{\mathrm{I}}$ defined for the notch. Recent research has shown that the value of $K_{\mathrm{I}}$ may be a controlling parameter for failure analysis of some materials (Dunn et al., 1997; Grenestedt and Hallstorm, 1997). The non-smooth BEM solutions converge to a value of 1.13 for $t_y^{\varphi}$ at the notch tip. Accurate determination of that same quantity for the FEM solutions is more problematic. However, rough estimates are clearly possible by extrapolating the smooth portion of the $t_y^{\varphi}$ distribution.

### 5.6. Plate with edge crack (fracture mechanics)

Computational mechanics analysts have worked on linear elastic fracture mechanics for a long time. All efforts have been concentrated on considering the singularity in finite element models by using a special element or modifying shape functions. Here we solve a fracture mechanics problem systematically by using the new methods. Consider the edge cracked plate displayed in Fig. 12 in plane strain condition. For the specific case considered the geometric parameters are established as $h = 5$, $w = 5$, $a = 1$ while the applied traction $t_0 = 1$. Material properties are again assumed to be $E = 1$ and $v = 0.3$. We solve the problem with the non-smooth finite element and boundary element methods. From the asymptotic expansion of Williams (1952), we know the singularity of stresses for free-free edges is $r^{-0.5}$. Because of symmetry of the body and loading we only need to use a single region method. On the cut crack edge we take $\varphi = r^{-0.5}$, while on the rest of the boundary $\varphi = 1$.

The problem is analyzed with our traction-oriented finite element and boundary element formulations and two levels of mesh refinement are examined for each method. The coarse mesh employs 50 quadratic

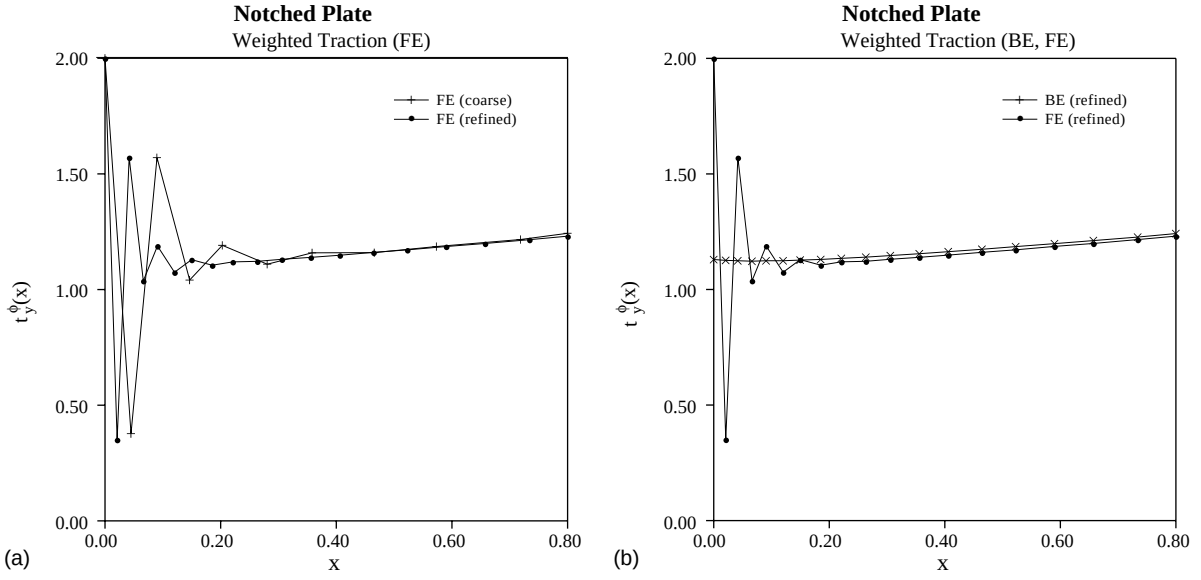


Fig. 11. Edge notch—numerical solutions.

elements along the boundary, while the refined model uses 106 elements. This corresponds to 200 and 412 degrees-of-freedom, respectively. An interior mesh is, of course, required in the FEM method. This consists of 221 eight-noded quadrilateral elements for the coarse mesh and 975 for the refined mesh. Again the boundary representation for the BEM and FEM analyses are identical.

Finite element results are presented in Fig. 13a. Nodal values of the weighted traction $t_y^{\varphi}$ are plotted versus distance from the crack tip as measured along the symmetry boundary. We see that the results have nearly converged away from the crack tip. Near the crack tip, the weighted traction oscillates with a significant amplitude. Figure 13b compares the $t_y^{\varphi}$ results obtained from the FEM and BEM refined meshes. Away from the crack tip, the BEM values for $t_y^{\varphi}$ are slightly larger than the FEM values. Near the tip, the present non-smooth BEM solutions are quite stable. From the results shown in Fig. 13b, we may estimate the weighted traction at the crack tip $t_y^{\varphi}(0)$. Of course, the formal stress intensity factor $K_{\mathrm{I}}$ is related to $t_y^{\varphi}(0)$ from the relation (e.g., Kanninen and Popelar, 1985)

$$K_{\mathrm{I}} = \sqrt{2\pi} t_y^{\varphi}(0)$$

For the non-smooth BEM refined mesh, we obtain $K_{\mathrm{I}} = 2.425$. This value is confirmed by additional analyses with further refinement. The determination of $K_{\mathrm{I}}$ for the FEM analyses is more difficult.

By using Williams's expansion (1952) we have

$$t_y(r) = \frac{1}{\sqrt{r}}(C_0 + C_1 r + C_2 r^2 + \cdots) = \frac{1}{\sqrt{r}} \sum_{k=0}^{\infty} C_k r^k$$

on the symmetry line. Therefore by definition $t_y(r) = \varphi(r) t_y^{\varphi}(r)$ with $\varphi(r) = r^{-0.5}$ we obtain

$$t_y^{\varphi}(r) = C_0 + C_1 r + C_2 r^2 + \cdots$$

where $C_0 = t_y^{\varphi}(0)$. Figure 13b suggests that we can approximate this distribution around the crack tip by the linear part

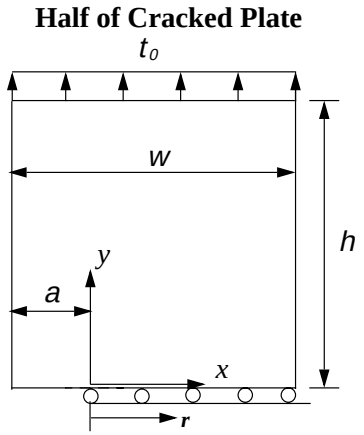


Fig. 12. Edge crack—problem definition.

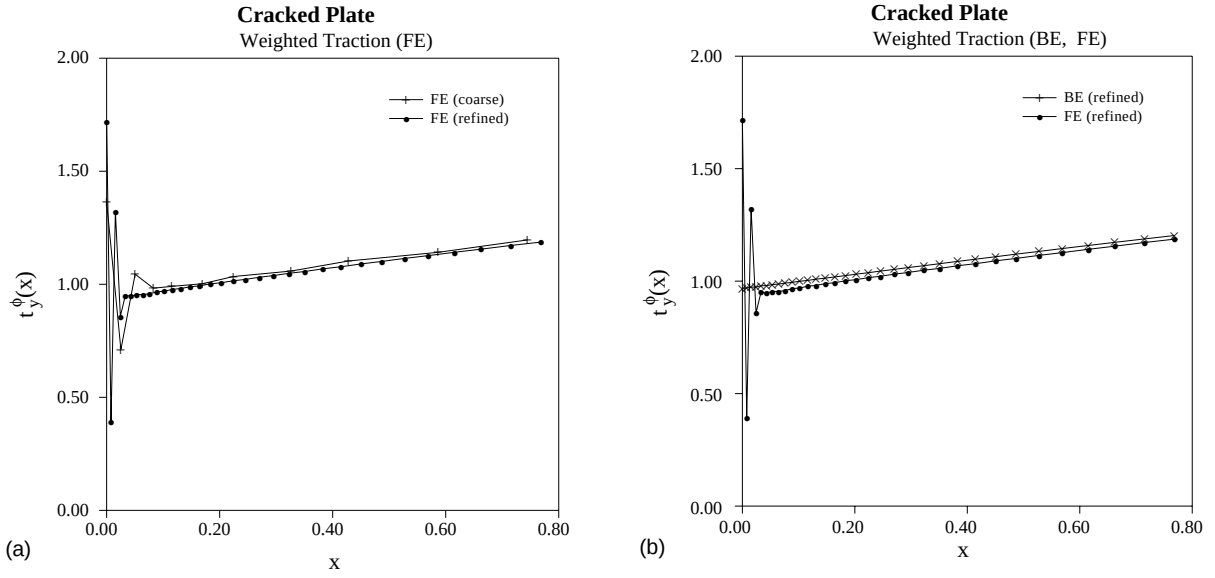


Fig. 13. Edge crack—numerical solutions.

$$t_y^{\varphi}(r) \approx C_0 + C_1 r$$

By excluding the first five nodes which are in the oscillating part and then using a simple least-square straight line curve fitting for the next four nodes, we find $K_{\mathrm{I}} \approx 2.35$ for the refined FEM model. Increasing the number of nodes for this curve fitting has little affect on the results. Meanwhile, we also performed a BEM analysis using quarter-point and traction-singular elements (Blandford et al., 1981). This yielded a stress intensity value $K_{\mathrm{I}} = 2.423$.

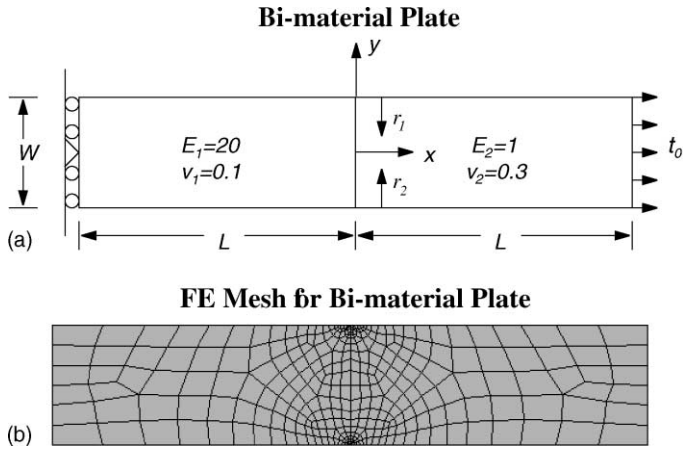


Fig. 14. Bi-material plate—problem definition.

### 5.7. Elastostatic problem for bi-material plate (composite materials)

In the previous examples, we considered non-smooth cases for notched and cracked bodies. Another example of non-smooth problems involves composite materials. Singularities can exist on the interface of two bonded materials.

It turns out that the stress state in the singularity dominated zone close to the corner of a non-cracked bi-material interfaces can be written (Bogy, 1971)

$$\sigma_{ij} = \sum_{m=1}^{\infty} \mathrm{Re}[Q_m r^{\gamma_m - 1} f_{ij}^m(\theta)]$$

where the eigenvalues $\gamma_m$ are roots to a special characteristic equation. These eigenvalues generally are complex as are also the stress intensity factors $Q_m$ and the functions $f_{ij}^m$. The most important eigenvalue is the one with the smallest real part fulfilling the requirement $\mathrm{Re}[\gamma_m] > 0$. Other terms will be ignored and we subsequently drop the index $m$. These stress intensity factors are generalized forms of $K_\mathrm{I}$ and $K_\mathrm{II}$ for ordinary cracks, or the complex stress intensity factors $K = K_\mathrm{I} + \mathrm{i}K_\mathrm{II}$ for cracks along bi-material interfaces.

We investigate the response of a bi-material plate within the context of plane strain elastostatic loading. The boundary value problem is defined in Fig. 14a. Solutions are obtained for $L = 5$, $W = 2$ with applied load $t_0 = 1$. The properties for the two isotropic material regions are specified as $E_1 = 20$, $v_1 = 0.1$ and $E_2 = 1.0$, $v_2 = 0.3$.

We solve the problem with the non-smooth traction-oriented finite element and boundary element methods. A total of 66 quadratic boundary elements and 264 degrees-of-freedom are used to model each region along the boundary. Continuity of displacements and tractions is enforced across the interface.

Table 5
BE analysis for bi-material plate

| $p$-type | Standard BEM stress $t_x(0)$ | Non-smooth BEM stress intensity $t_x^\varphi(0)$ |
|---|---|---|
| Linear | 3.70 | 0.70 |
| Quadratic | 4.53 | 0.70 |
| Quartic | 5.65 | 0.70 |

A total of 20 boundary elements model this interface. An interior mesh is, of course, required in the FEM method. This consists of 157 eight-noded quadrilateral elements for each domain as shown in Fig. 14b.

The result of standard BEM for $t_x$ is a finite value, which increases by using finer meshes. The value of $t_x$ on the interface at the upper free edge has been computed with a standard boundary element analysis. A series of $p$-refinements are performed to investigate the convergence characteristics as the order of the element functional variation is increased. We see from the results in Table 5 that the value of $t_x$ at the mentioned point increases with refinement. Further refinement beyond this cannot improve the situation.

Based upon the local analysis, we already know $t_x$ is infinite on this interface at the intersection with the free boundary. By introducing a proper weighting function, the boundary value problem can be solved completely in terms of bounded quantities. Since there are actually two singular points, the weighting function is chosen as the product $\varphi = \varphi_1\varphi_2$, where

$$\varphi_1 = \frac{1}{r_1^{1-\gamma}}$$

$$\varphi_2 = \frac{1}{r_2^{1-\gamma}}$$

with $r_1$ and $r_2$ as the radial distances defined in Fig. 14a. From the analytical asymptotic solution for an infinite bi-material wedge, $\gamma \approx 0.7595$ (Bogy, 1971).

The results of the traction-oriented FEM and non-smooth BEM for $t_x^{\varphi}$ at the free edge on the interface are shown in Fig. 15 and Table 5. It is seen that there is a good correlation between the BEM results. However, additional assumptions are needed to estimate the generalized intensity factor $\boldsymbol{t}^{\varphi}(0)$ from the oscillating FEM solutions. Recent research suggests that the values of $\boldsymbol{t}^{\varphi}(0)$ be useful in the failure analysis of some interfacial joints (Reedy and Guess, 1997). Therefore, systematic methods for determining $\boldsymbol{t}^{\varphi}(0)$ may prove to have some importance.

## 6. Concluding remarks

The theory of fundamental eigensolutions gives a new view to the theory of elastostatic boundary value problems and their numerical solution. A spectral analysis of the direct boundary element method and a traction-oriented finite element method is provided for the first time. The solution to boundary value problems is then seen as an indirect generalized discrete Fourier analysis. Furthermore, the numerical formulations based upon boundary element and finite element methodologies that have been developed here remain valid even for non-smooth problems associated with notches, cracks and mixed boundary conditions. This was illustrated in several examples presented in Section 5. Most mathematical models of practical engineering problems are non-smooth. For example, mixed boundary conditions may be specified, re-entrant corners may be present or bi-material interfaces may exist. Consequently, we believe that these formulations should be given serious consideration.

In order to summarize, we now reiterate a few of the other important ideas associated with these computational methods. Recall that both finite element and boundary element solutions can be written as the linear combination of the first $N$ (approximate) eigenmodes. The number of these eigenmodes in a discretized finite element model relates to the number of boundary nodes, not to the number of interior nodes. Of course, no internal nodes exist in a boundary element model. We conclude that the number of degrees-of-freedom $N$ in the discretized version of the boundary value problem in both models is determined by the number of boundary nodes $N_B$ and the dimensionality of the problem $d$. Interior nodes in a finite element model only help to improve the accuracy of the fundamental eigenmodes. In traditional finite

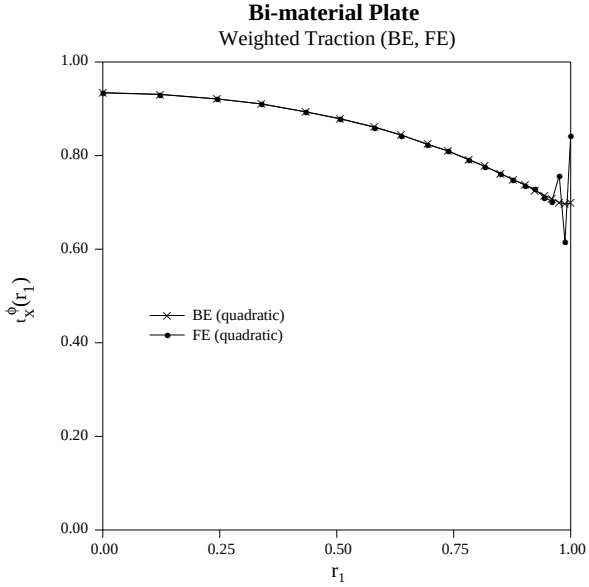


Fig. 15. Bi-material plate—numerical solutions.

element methods, all nodes are included in determining the degrees-of-freedom, however this is not consistent with the theory of fundamental eigensolutions. More appropriately the number of degrees-of-freedom is equal to the number of fundamental eigensolutions (i.e., $N = N_B d$). Furthermore, with this interpretation, it may be possible to obtain a better theoretical understanding of the phenomenon of locking and related empirically-based patch tests.

We should again mention that the eigensolutions in the finite element method are more approximated than the eigensolutions in the boundary element method for the same boundary nodes. Notwithstanding, the finite element eigensolutions are always real and orthogonal, while those in the boundary element method usually are not orthogonal. Some modes in BEM might be complex, which is a potential source of instability.

In non-smooth problems, using the proper weight function $\varphi$ to make $\boldsymbol{t}^{\varphi}$ piecewise regular has several advantages. Most importantly, calculations are then based on bounded functions. Additionally, the Fourier coefficients $\tilde{A}_n$ decrease faster for higher modes. This means that the participation of higher modes are less important than for the case with $\varphi = 1$. Consequently we may expect higher quality solutions for a given mesh when $\varphi$ is chosen properly. The non-smooth boundary element solutions provided in Section 5 illustrate the high level of accuracy that is attainable. On the other hand, further research is needed to improve the quality of the finite element solutions for non-smooth problems. One can, of course, also utilize the formulations presented here to effectively combine boundary element and finite element methods in a single analysis by employing a multi-region approach.

In this paper, we have explored the practical impact of the theory of boundary eigensolutions on the finite element method and the boundary element method as well as their interrelationship. This theory also provided explanation of some important concepts, including convergence and degrees-of-freedom in a robust mathematical manner. This is not restricted to the finite element and boundary element methods presented here. Every computational elastostatic formulation follows this theory. Furthermore, within the context of the theory of boundary eigensolutions, every computational mechanics method can be con-

ceptualized as an indirect generalized discrete Fourier analysis method. We say that it is indirect, because we usually do not need to find eigensolutions to solve a boundary value problem.

Part I and II together provide a new perspective for the study of elastic boundary value problems. The presentation focused on elastostatic problems and only two-dimensional examples were provided. However, the methodology is not at all restricted in this way. The theory applies directly to three-dimensional elasticity and to more general classes of boundary value problems.

## References


Aliabadi, M.H., Rooke, D.P., Cartwright, D.J., 1987. An improved boundary element formulation for calculating stress intensity factors: Application to aerospace structures. J. Strain Anal. 22, 203–207.

Anderson, E. et al., 1992. LAPACK User's Guide. SIAM Publishing, Philadelphia.

Banerjee, P.K., 1994. The Boundary Element Methods in Engineering. McGraw-Hill, London.

Barone, M.R., Robinson, A.R., 1972. Determination of elastic stresses at notches and corners by integral equations. Int. J. Solids Struct. 8, 1319–1338.

Barsoum, R.S., 1975. Further application of quadratic isoparametric finite elements to linear fracture mechanics of plate bending and general shells. Int. J. Fract. 10, 167–169.

Bathe, K.J., 1996. Finite Element Procedures. Prentice-Hall, Englewood Cliffs, NJ.

Blandford, G.E., Ingraffea, A.R., Liggett, J.A., 1981. Two dimensional stress intensity factor computations using the boundary element method. Int. J. Numer. Meth. Eng. 17, 387–404.

Bueckner, H.F., 1970. A novel principle for the computation of stress intensity factors. Z. Angew. Math. Mech. 50, 529–546.

Bogy, D.B., 1971. Two edge-bonded elastic wedges of different materials and wedge angles under surface tractions. J. Appl. Mech., ASME 38, 377–386.

Cruse, T.A., 1969. Numerical solutions in three dimensional elastostatics. Int. J. Solids Struct. 5, 1259–1274.

Cruse, T.A., Van Buren, W., 1971. Three dimensional elastic stress analysis of a fracture specimen with an edge crack. Int. J. Fract. 7, 1–15.

Dunn, M.L., Suwito, W., Cunningham, S., 1997. Stress intensities at notch singularities. Eng. Fract. Mech. 57, 417–430.

Grenestedt, J.L., Hallstorm, S., 1997. Crack initiation from homogeneous and bimaterial corners. J. Appl. Mech., ASME 64, 811–818.

Gunn, M.J., Britto, A.M., 1984. CRISP User's and Programmer's Guide. Engineering Department, Cambridge University.

Hadjesfandiari, A.R., 1998. Theoretical and computational concepts in engineering mechanics. Ph.D. Dissertation. State University of New York at Buffalo.

Hadjesfandiari, A.R., Dargush, G.F., 2001a. Boundary eigensolutions in elasticity. I. Theoretical development. Int. J. Solids Struct. 38, 6589–6625.

Hadjesfandiari, A.R., Dargush, G.F., 2001b. Theory of boundary eigensolutions in engineering mechanics. J. Appl. Mech., ASME 68 (1), 101–108.

Hadjesfandiari, A.R., Dargush, G.F., 2001c. Computational mechanics based on the theory of boundary eigensolutions. Int. J. Numer. Meth. Eng. 50, 325–346.

Henshell, R.D., Shaw, K.G., 1975. Crack tip finite elements are unnecessary. Int. J. Numer. Meth. Eng. 9, 495–507.

Kanninen, M.F., Popelar, C.H., 1985. Advanced Fracture Mechanics. Oxford University Press, New York.

Paris, P.C., McMeeking, R.M., Tada, H., 1976. The weight function method for determining stress intensity factors. In: Swedlow, J.L., Williams, M.L. (Eds.), Cracks and Fracture: Proceedings of the Ninth National Symposium on Fracture Mechanics. ASTM, pp. 471–489.

Press, W.H., Teukolsky, S.A., Vetterling, W.T., Flannery, B.P., 1992. Numerical Recipes in Fortran. Cambridge University Press, Cambridge, UK.

Reedy Jr., E.D., Guess, T.R., 1997. Interface corner failure analysis of joint strength: Effect of adherend stiffness. Int. J. Fract. 88, 305–314.

Rizzo, F.J., 1967. An integral equation approach to boundary value problems of classical elasto-statics. Q. Appl. Math. 25, 83–95.

Snyder, M.D., Cruse, T.A., 1975. Boundary integral equation analysis of cracked plates. Int. J. Fract. 11, 315–328.

Symm, G.T., 1973. Treatment of singularities in the solution of Laplace's equation by an integral equation method. National Physical Laboratory Report NAC31.

Williams, M.L., 1952. Stress singularities resulting from various boundary conditions in angular corners of plates in extension. J. Appl. Mech., ASME 19, 526–528.